Student thesis series INES nr 497

# Energy balance closure, water balance, carbon exchange, and water use efficiency: observed and modeled outcomes for a managed, hemiboreal forest in Southern Sweden

**Linsey M. Avila**

2019
Department of
Physical Geography and Ecosystem Science
Lund University
Sölvegatan 12
S-223 62 Lund
Sweden

Linsey M. Avila
***Energy balance closure, water balance, carbon exchange, and water use efficiency: observed and modeled outcomes for a managed, hemiboreal forest in Southern Sweden***
Master degree thesis, 30 credits in *Physical Geography and Ecosystem Analysis*
Department of Physical Geography and Ecosystem Science, Lund University

Level: Master of Science (MSc)

Course duration: *January* 2018 until *August* 2019

Disclaimer

# Energy balance closure, water balance, carbon exchange, and water use efficiency: observed and modeled outcomes for a managed, hemiboreal forest in Southern Sweden

Linsey M. Avila

Master thesis, 30 credits, in *Physical Geography and Ecosystem Analysis*

Thesis Supervisor:
Harry Lankreijer, PhD
Lund University, Department of Physical Geography & Ecosystem Science

Exam Committee:
David Tenenbaum, PhD
Lund University, Department of Physical Geography & Ecosystem Science

Maj-Lena Linderson, PhD
Lund University, Department of Physical Geography & Ecosystem Science

## ABSTRACT

Energy, water, and ecosystem level carbon biosphere-atmosphere exchange were examined over a two-year study period from January of 2015 to December of 2016 at a managed forest site in southern Sweden. The energy balance was initially evaluated for closure, and to see which energy components had the largest influence on this system. Initial energy balance closure before energy storage correction was 0.75 and improved by about twenty percent after energy storage was modeled. Shortcomings in the energy balance were outlined by looking at closure during varying atmospheric conditions. The best EBR values prior to correction happened during daytime hours when friction velocities were higher than 0.8 m $s^{-1}$ and windspeeds were higher than 4 m $s^{-1}$ for stable-neutral and unstable conditions. Closure of the energy balance was then used to validate later calculations of evapotranspiration. Substantiated evapotranspiration fluxes were used to determine the nature of the water balance and water use efficiency. Looking at the water balance revealed the extent of the drought that occurred in 2016, which had less precipitation and higher temperatures than 2015. Temporal investigation of the individual water balance components described when the drought was most severe and which components were most affected. This decrease in incoming water had the largest effect on soil water storage and ground water storage. Diurnal patterns for the radiation components, evapotranspiration, $CO_2$ fluxes and ecosystem exchanges were then evaluated. All of which were highest during daytime hours of the growing season. Integrated water use efficiency at the ecosystem level was determined and productivity of carbon sequestration for biological growth was gauged. Water use efficiency and the carbon exchanges indicated high productivity during the study period primarily during daytime hours of the growing season when the forest acted as a carbon sink. During nighttime and non-growing season periods it released more carbon than it took up. Aggregate, annual gross primary production was surprisingly higher in 2016 at 291 g C m-2 year-1, which was unexpected given the environmental strain placed upon this ecosystem due to drought stress. The implications of this suggest that drought stress would need to be more severe to make a lasting, negative effect on forest productivity.

Keywords: Energy balance, energy balance closure, energy balance ratio, net radiation, sensible heat, latent heat, turbulent fluxes, ground heat flux, energy storage, available energy, Bowen ratio, evaporative fraction, latent heat of vaporization, water balance, evapotranspiration, precipitation, water storage, water discharge, gross primary production, ecosystem respiration, net ecosystem production, carbon exchange, water use efficiency

Table of Contents

# 1. INTRODUCTION

The claims for the potential of boreal and sub-boreal forests to combat negative effects of climate change have been substantial with over half of Earth's primary forest in boreal and temperate regions of the Northern Hemisphere. These forests alone are responsible for about a $1.3 \pm 0.5$ gigaton uptake of carbon per year (Luyssaert et al. 2008). However these arctic and subarctic forests' combined affinity for $CO_2$ sequestration as a large global carbon sink (Pan et al. 2011) could be offset by lowered surface albedo warming effects (Betts 2000, Bonan 2008) and current and future land use change (Myneni et al. 2001).

It is for these reasons that the health and continued maintenance of these systems are important, since they will ultimately determine which climate predictions are most probable in coming years. According the Artic Monitoring and Assessment Program (2013), the observed mean annual air temperature within arctic and subarctic regions has increased two-fold in comparison to the rest of the world. Positive feedbacks in the form of earlier annual sea ice and snow melt leading to increased absorbed soil and vegetation radiation could further perpetuate these rises in air temperature (Tang, 2014) creating a vicious cycle for Earth's climate. This stronger winter warming, and prolonged growing seasons have already been observed in recent years (Xu et al. 2013). While a greener arctic and subarctic could result in a climate cooling effect by increasing boreal carbon sequestration, the warming effects from decreased surface albedo due to reduced snow cover and sea ice (Snyder 2013) could offset these cooling, negative feedback loops. Given the likely occurrence of more extreme climate events in the future (IPCC 2015), ascertaining a better understanding of how climate effects, such as profound fluctuations in precipitation, decreases in yearly snow, faster snow melt rates, variability in evapotranspiration due to environmental stress, and related changes in hydrological and carbon cycles will change these northern, boreal landscapes in critical ways.

These landscapes also house the potential for other climate mitigation schemes, one of which being virtual water trade. Increasing managed forest land-use in water rich environments would increase productivity for lumber industries as it takes far less water to produce the same amount of lumber in water rich environments than in semi-arid and arid regions where water is far more scarce (Kumar and Jain 2008, Hoekstra and Hung 2003). This increase in industry efficiency has big implications for global anthropogenic water consumption as water supply issues are being further exacerbated with growing global demand of water. A shift away from crop and lumber production in water poor environments would lower the necessity for diverting water to these regions, as well, and instead diverted water could be used almost exclusively for meeting direct human consumption needs. However, some issues with this do arise as global landscapes shift and annual inputs for water change location. Maintaining optimal water security will require an adaptive approach with mobile land-use application dependent on annual water inputs, which require continued research on the everchanging location of high rain-fed environments due to climate change.

In order to accurately evaluate how these boreal, hemiboreal, and boreal bordering landscapes will change in the future the environmental conditions within these systems must be better understood. Every environment is made up of a myriad of features that ultimately regulate the spatial dissemination of hydrological, carbon, and energy processes. Rates of soil recharge, discharge, evapotranspiration, and overall ecosystem productivity from biological

growth depend on these varying environmental factors (Andersson, 1989). Without determining how these sub-arctic systems react to changes over time it is hard to establish what will come next. The closer one gets to accurately defining the underlying mechanisms that drive a system, the more realistic the current and future experimental assessments will be. Fortunately, the measurement data available for these landscapes continues to grow, making the possibilities for extensive and globally robust research even more conceivable over longer longitudinal periods of time.

## 1.1 Study Aim

The scope of this study, over the course of a two-year study period from January of 2015 to December of 2016, will be to run a general quality check for the measurements taken at a newly established research station. This will start with defining the available energy present within system and see how this drives the turbulent fluxes from at the forest surface. The water balance will also be studied to see if there were any sizeable effects on the other underlying processes within this environment. Lastly, the water use efficiency and overall forest productivity will be evaluated to gain a better understanding how prolific these systems can be in their ability for $CO_2$ uptake and forest productivity. From a larger perspective, the purpose of this research will be to better comprehend how forest ecosystems, like the one present at this study site, could support efforts to combat the negative effects of climate change, and inversely how the changing climate will in-turn effect these environments over time.

The energy storage fluxes will be mathematically modeled to fill gaps in energy balance closure. The discrepancy between available energy and the turbulent fluxes is significant. If the storage energy fluxes are calculated accurately, they should substantially reduce the disparity between available energy and the turbulent latent and sensible heat fluxes ultimately resulting in an improved energy closure ratio much closer to a value of one (Moderow et al. 2009). The closer these models get to achieving energy balance closure the better they will support the first law of thermodynamics, which states the conservation of energy. Diurnal cycles for all energy components will be graphically described to depict patterns in daily energy fluxes, and a special look at the turbulent fluxes of sensible and latent heat will provide more insight into the exact nature of surface energy fluxes at this specific location over the study period (Lewis 1995). Verified latent heat flux measurements will then be used to calculate rates of evapotranspiration for both the water balance and water use efficiency analysis. The forest water balance over the course of the study period will better explain short term effects on the individual water components during times of drought and water abundant conditions (Jones et al. 2017). This will include water storage response to fluctuating inputs of water in the form of precipitation and snowfall with maintained rates of evapotranspiration (ET). An individual look at evapotranspiration during times of normal and environmentally stressful circumstances will supplement the current understanding of vegetal physiological processes over the course of the two-year study period (Pidwirny and Jones 2006).

An in-depth look at the carbon balance, more specifically, gross primary production (GPP), ecosystem respiration ($R_{eco}$), and net primary production (NEP), will help to further explain the underlying physical and chemical processes of the forest site during varying environmental conditions over the course of the two-year study period (Ilvesniemi et al. 2009). Average diurnal cycles for GPP, ET, and water use efficiency (WUE) during the course of the entire year and only the growing seasons will hopefully deliver a detailed account of peak forest productivity, as well as, a better

understanding of daily patterns as a whole (Tang et al. 2015, Xuguang et al. 2014). Overall forest productivity for the study period will be determined by looking at monthly WUE from rates of GPP to ET, as well as, identifying temporal accumulative changes in the three carbon exchanges: GPP, $R_{eco}$, and NEP (Beer et al. 2007, Ponton et al. 2006, Scartazza et al. 2014). A special look at $CO_2$ flux densities at differing temporal scales will allow for a better understanding of this managed forest's ability to sequester $CO_2$, with special attention placed on the differences between the two study years. This will give a rough insight into this hemiboreal forest's ability to combat the rising, negative effects of climate change on the global environment.

### 1.2 Research Questions

(1) How will modeled energy storage corrections improve the energy balance closure issue at this study site?
   a. Analyze the energy balance pre-correction as an initial quality check for measured energy flux observations.
   b. What will modeled energy correction look like for the individual energy components?
   c. Define the character of the surface turbulent fluxes, primarily latent heat, for use later in the study.

(2) How does the water balance, and individual water balance components, respond to surplus precipitation versus drought conditions?
   a. What does this look like at different temporal scales?

(3) How do the carbon exchanges, as well as water use efficiency, respond to environmental stress in terms of prolonged drought?
   a. When is this study site predominantly a carbon source, and when does it act as a carbon sink?
   b. How does time of day, time of year, incoming light, and ambient temperature affect these exchanges?

## 2. BACKGROUND

### 2.1 Energy

The Earth's energy balance is the equilibrium between incoming sun energy and outgoing terrestrial energy from the earth's surface. Some of the energy released from the sun reaches earth as shortwave radiation where it is then either reflected back off of clouds, absorbed into the atmosphere, or at Earth's surface. The energy attained from the sun in theory is in constant balance with the terrestrial energy lost from the Earth's surface in the form of shortwave and longwave radiation. It is this balance that regulates and preserves the temperature patterns we see, and the predictable climates that we know here on Earth.

### 2.2 Water

Similarly the hydrological cycle, is the constant circulation of water within the Earth-atmosphere system. Of the countless processes within this cycle, the most often discussed components are precipitation, condensation, evaporation, transpiration (together evapotranspiration), water discharge or runoff above and below the Earth's surface, percolation, and condensation.

### 2.3 Carbon

The carbon cycle refers to the biogeochemical exchanges of carbon within all four of Earth's spheres. This includes the dynamic exchanges of $CO_2$ and other carbon containing molecules between the biosphere, lithosphere, hydrosphere, and atmosphere. This cycle is regulated by the physical and chemical properties present within the given medium, and incredibly important here on Earth as carbon is the basic building block for all life as we know it. Without carbon, life on Earth would cease to exist.

Table 1. Climatic, geographic and soil characteristics for ICOS Hyltemossa provided by ICOS (2018) and the Swedish Meteorological and Hydrological Institute (SMHI, 2018).

| Site information | ICOS Hyltemossa |
|---|---|
| Storm damage or clear cut | 1981, 1982 |
| Replanted | 1983 |
| Cleaned or thinned | 1998, 2005, 2009, 2013 |
| Research station founded | 2014 |
| Location | N 56.0976◦ E 13.4190◦ |
| Elevation (meters above sea level) | 104 |
| Primary tree species | Norway spruce (Picea abies) |
| Forest density pre-thinning (stems hectare$^{-1}$) | 3300 |
| Forest management turnover (years) | ~50 |
| Estimated, unimpeded stem growth (meters) | 34 |
| Study period average stand height (meters) | 19 |
| Average stand density ($m^3$ hectare$^{-1}$) | 190 |
| Average 50-year mean annual temperature (°C) (SMHI) | 7.2 |
| Average 50-year total annual precipitation (millimeters) (SMHI) | 765 |
| Average 50-year total annual snow depth (meters) (SMHI) | 3.4 |
| Soil classification | Cambisol with some podzol |
| Soil texture | Sandy till, glaciofluvial sediment |

## 2.4 Measurement Acquisition

The predominant measurement method used for most of the variables explored in this study were obtained through the eddy covariance method. This method is a micro-meteorological approach to observing exchanges of momentum, wind characteristics, energy, and gas fluxes between the ecosystem below the measurement system and the surrounding atmosphere. With its wide-ranging scope of application this method is highly coveted within the meteorological community. These systems typically consist of a two-part instrumentation that includes an infrared gas analyzer (IRGA) and a sonic anemometer. These two together are able to measure these flux exchanges recording measurements ten to thirty times every second and then calculating the covariance per second between the deviation in instantaneous vertical windspeed (w) and mean instantaneous deviation in the concentration of the measured variable. For all the ecosystem exchanges, $CO_2$ fluxes, and turbulent fluxes, as well as all of the wind characteristics were measured by this method.

Other measurement methods used at the study site include pyranometers for radiation, temperature probes for differing temperature readings, ground heat flux plates placed below the ground surface, theta probes for volumetric water content, rain gauge for precipitation, sonic ranging sensor for snow depth, digital barometer for atmospheric pressure, and a pressure transducer for ground water levels.

# 3. DATA AND METHODS

## 3.1 Site Description

The Hyltemossa site, established in 2014, lies roughly 6.5 kilometers South of the Perstorp municipality in the Northwestern part of Skåne County in Southern Sweden, and serves as a dual atmosphere and ecosystem measuring station for the Integrated Carbon Observation System (ICOS) Sweden Network. The station stands within a 30-year old, managed boreal forest consisting almost entirely of Norwegian

Spruce (*Picea abies*) with small openings of mixed deciduous birch trees (*Betula sp.*) and Scots pine (*Pinus sylvestris*).

While it lies within the nemoral region of Scandinavia (Diekmann 1994), the more boreal leaning site characteristics make it currently possess characteristics that are typically more hemiboreal or boreo-nemoral in nature. Since there is a greater representation of boreal than temperate species present and the climatic conditions often fall within the middle ground of nemoral and boreal at this forest site the hybrid classification serves best (Teuling 2011, Rubel and Kottek 2011). However, this classification is likely subject to change with the changing climate, where it is likely to possess more temperate properties, as predicted in global climatic classification models (Kottek et al. 2006, Rubel and Kottek 2010).

Pocketed between several small lakes (Figure 1) to the North, East, and South, the Hyltemossa area feeds a substantial amount of its annual discharge into the neighboring Rönne Å River that lies 13 kilometers to the West each year. On average Hyltemossa experiences humid conditions, usually receiving globally far above average volumes of precipitation each year (IPCC 2015). Table 1 expresses typical annual conditions based off of fifty-year averages from a nearby meteorological station for this study site, where annual temperature and rainfall obtained from SMHI show support for the mapped climatic predictions made by IPCC.

## 3.2 Instrumentation & Site Conditions

All meteorological data came directly from the station tower at varying heights. Ecological and hydrological data was either measured directly from the tower, or within 200 meters of the tower. Full descriptions of variables used, with their measurement heights, and instrumentation can be found in Table A of the appendix. For clarity, Table B in the appendix lays out which variables were measured, and which were mathematically modeled along with their corresponding units and converted units if applicable.

Before diving into the energy, water, and carbon flux analysis general site conditions were described. This included: digital elevation modeling with hydrological features represented within the study area, spatially modeled flux footprint analysis for the entirety of the study period, computed surface albedo from incoming, S↓, and outgoing shortwave radiation, S↑, (Equation 1), and vapor pressure deficit, VPD, (Equation 2, 3, & 4) where VPD was the difference between saturated vapor pressure ($e_s$) and actual vapor pressure ($e_a$).

$$Albedo = \frac{S\uparrow}{S\downarrow} \quad (1)$$

Measured variables of precipitation, temperature, photosynthetically active radiation (PAR), and relative humidity (RH) were temporally defined for annual patterns within the study period. Values for relative humidity and the calculated vapor pressure deficit, dependent on relative humidity, started in June of 2015, as measurements for this were not collected until that time.

$$e_s = 610.7 \times 10^{7.5\mathrm{T}/(237.3+\mathrm{T})} \quad (2)$$

The saturated vapor pressure function is temperature dependent (T), as seen in Equation 2.

$$e_a = \frac{RH \times e_s}{100} \quad (3)$$

Actual vapor pressure was derived from the calculated saturated vapor pressure and measured relative humidity (Equation 3). Vapor pressure deficient was the difference between saturated vapor pressure and actual vapor pressure (Equation 4).

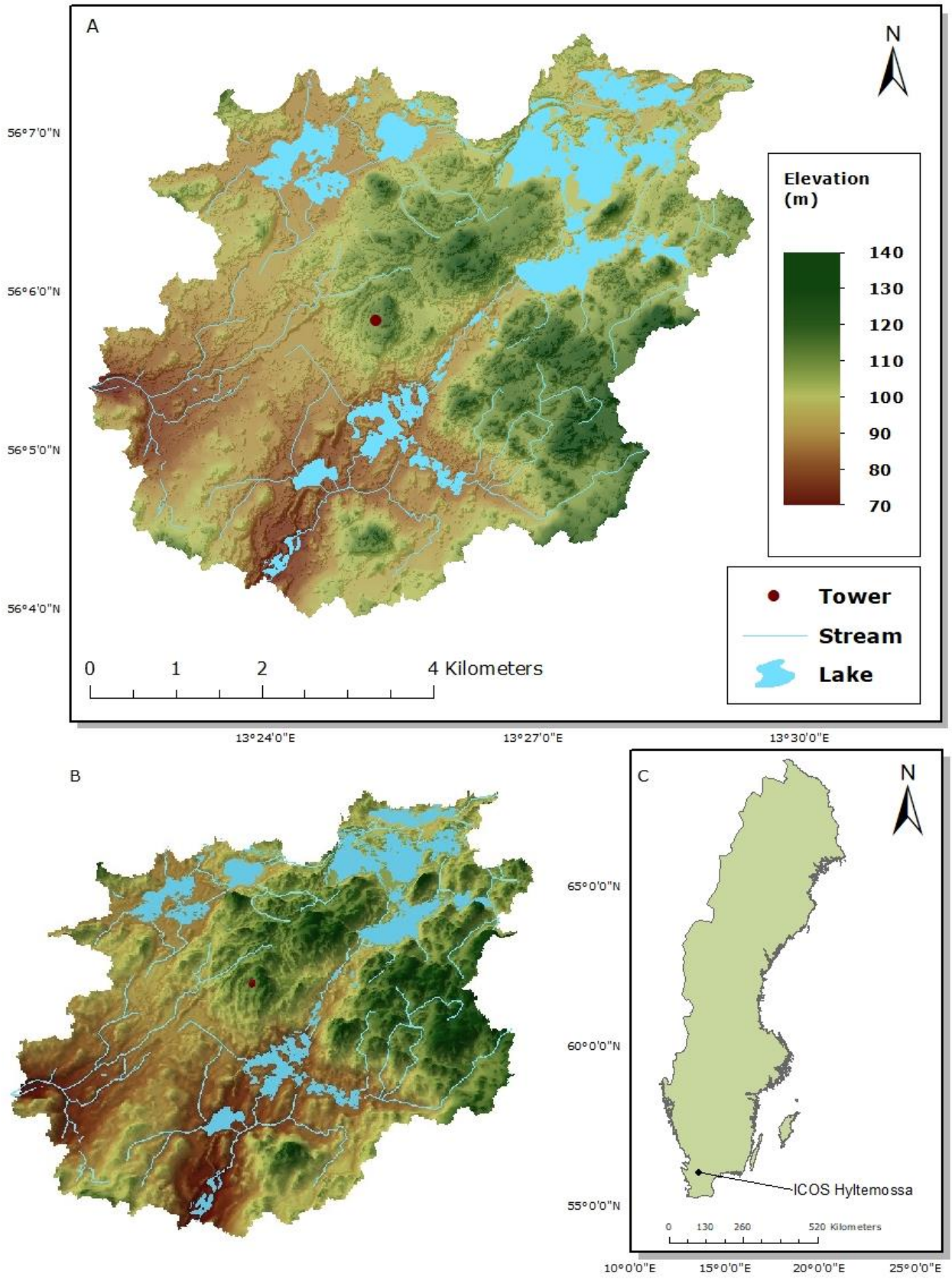


Figure 1. Digital elevation maps created using the Swedish National Land Survey (Lantmäteriet) LiDAR data 1A shows the elevation of the Hyltemossa Research Station and surrounding area, with lakes and streams shown in blue, and a red dot indicating the tower location 1B is the same DEM rotated in ArcScene from a southwest angle to better show dominant flow direction, and 1C a map of Sweden with a pinned location for the ICOS Hyltemossa Research Station.

$$VPD = e_s - e_a \quad (4)$$

To spatially model the flux footprint the Kljun et al (2015) flux footprint prediction (FFP) model simulator was chosen, which utilized calculated zero-plane displacement height (m) and surface roughness lengths (m), as well as, observed measurement height (m), wind direction in degrees ($360^{\circ}$) for rotation of the footprint, mean wind speed at the designated measurement height ($ms^{-1}$), the standard deviation of lateral velocity fluctuations after rotation ($ms^{-1}$), the friction velocity ($ms^{-1}$), and Obukhov length (m) to express the 2D flux radii for the study period. The simulator superimposed the flux radii contour lines onto a satellite image of the study site. Land-use classification was spatially modelled from the satellite image to depict the percentages of differing land-use classes within the flux radii. These classes included spruce dominated coniferous forest, mixed deciduous forest, build-up area, semi-natural grassland, and croplands.

Wind characteristics were rendered on a wind rose. Atmospheric stabilities ($\xi$) were calculated in Equation 5 for energy balance ratio analysis, where z refers to measurement height, d is the zero-plane displacement height, or 0.63 the canopy height, and L is the Obukhov length. Frequency percentages in histograms for friction velocity, wind speed and atmospheric stability were made to show the distribution of these conditions at the forest site during the study period.

$$\xi = \frac{z-d}{L} \quad (5)$$

## 3.3 Energy Balance Closure

The driving force behind the energy balance is net radiation ($R_n$). It is the residual energy left over after reflected longwave and shortwave radiation are removed from a given system (Equation 6).

$$R_n = S\downarrow - S\uparrow + L\downarrow - L\uparrow \quad (6)$$

Here S↓ represents downwelling shortwave radiation and S↑ reflected shortwave radiation. Longwave downwelling radiation is L↓ and longwave upwelling radiation is L↑ to leave the sum, $R_n$ as the final net radiation left in that given point in time. This balance has been at the center of many research campaigns for quite some time, and the general consensus has been that there is a need for measurement of these separate parts in order to determine the most accurate result (Sellers et al. 1997).

To authenticate $R_n$ used in later calculations, these energy components measured by ICOS Sweden were initially defined by Equation (6). A linear regression measured net radiation on the x-axis and the sum of the individually measured short and longwave radiative fluxes on the y-axis, with a corresponding $r^2$ value was used to access the degree to which these parts were balanced for the whole time series. In addition, quality control flags designated by the ICOS data preprocessing team helped access which points were erroneous and should be removed from processing entirely. Data with QC flags of 0, i.e. no error, were deemed fair to use, QC of 3, i.e. suspicious, were evaluated to determine if data points appeared to be clearly inaccurate or not, and QC flags of 9, i.e. missing or failed sensor, were removed all together. Gap-filled data, with a QC of 1, were used later in the analysis. This quality control designation was applied to all measured input variables in this study.

$$R_n = H + LE + G + J \quad (7)$$

Once measurements of $R_n$ were deemed suitable for use Equation (7) was investigated, where H is the turbulent sensible heat flux, LE is the turbulent latent heat flux, G is the ground heat flux, and J is the energy storage change in the canopy biomass and surrounding air.

This equation can be rewritten to express available energy with $R_n$ minus G and J on the left, and the turbulent fluxes, which reallocate this available energy (AE) back to the atmosphere, on the right. When LE and H fluxes are positive this energy is directed away from the canopy surface. Inversely, when storage is positive it indicated energy is maintained within the system below the flux measurement height.

*3.3.1 Preliminary Energy Flux Correction*

The remaining variables from Equation (7), aside from storage were checked for QC values before initial energy balance closure could move forward. From here initial energy balance closure was explored by comparing H+LE to Rn-G with a linear regression and $r^2$ and RMSE scoring. The slope of this initial energy balance indicated how large the gap in the energy closure would be before storage fluxes could even be determined. This was done for both pre and post gap-filled turbulent fluxes to govern which set, gap-filled or unfilled turbulent fluxes, were used later on in the study.

Following this initial look at energy closure, the total ground heat flux (G) was corrected by Equation (8). This included storage of heat through the soil profile below the surface ($G_s$) and measured at the surface ($G_z$) by heat flux plates. Storage change was derived from the soil volumetric heat capacity ($C_s$) and the average soil temperature ($T_s$) through the profile ($\Delta z$) over time (t) (Sauer and Horton 2005) . Specific heat as a function of soil moisture and constant specific heat were compared. Both yielded similar results, so the constant $C_s$ was eventually chosen for Equation (8). Since the soil thermal conductivity increases as a power function of soil moisture, while changes in the heat capacity are relatively infinitesimal (Liu, Wang and Fu 2008, Roxy, Sumithranand and Renuka 2014), a constant heat capacity proved perfectly suitable for this soil heat flux correction.

$$G = G_z + G_s = G_z + C_s \left(\frac{\delta Ts}{\delta t}\right)\Delta z \qquad (8)$$

*3.3.2 Modeled Energy Storage Fluxes*

There were no direct measurements for storage fluxes, so these had to be calculated by Equation (9) defined in several varying ways depending on authorship (McCaughey and Saxton 1988, Nordbo et al. 2011, Oliphant et al. 2004, Pan et al. 2017, Seibert et al. 2015, Barr et al. 2006). The calculation of storage (J) can essentially be boiled down to the modified Equation shown here.

$$J = J_H + J_E + J_s + J_c \quad (9)$$

For sensible heat storage ($J_H$) the temperature profile summation Equation (10) was further simplified since a sizeable amount of the temperature profile data for 2015 and some of 2016 was unfortunately invalid. Because measurement equipment was still being installed, and calibrated, a single temperature height was used. This was treated as one large layer to represent the whole temperature profile below. Where $\rho_a$ is air density, specific heat of air is $c_p$, and $T_a$ was the change in temperature over change in time ($\Delta t$) at height z.

$$J_H \cong \rho_a c_p \sum_{i=1}^{i=n} \frac{\Delta Ta,i}{\Delta t} \Delta z_i \qquad (10)$$

Similarly, the specific humidity profile had issues with continuity in data validity. Since this was the first year that measurements were taken at this research station, it could be expected. When installing measurement equipment that is to run continuously for decades, it is best to make sure everything is calibrated and running smoothly before logging data for public use. Thus many points were quality flagged by ICOS, and rendered unusable for this storage flux calculation. The latent heat storage ($J_E$) Equation (11) also had to be amended in a similar fashion to the sensible heat storage, where humidity was obtained and implemented for one single, large layer. Latent heat of vaporization as a function of

temperature (λ) was used in place of air density and specific heat, and absolute humidity, or simply vapor density ($\rho_v$) in place of temperature. The latter variable was obtained from relative humidity measurements, which established actual and saturated vapor pressures. The ideal gas law was then employed to define these 30-minute values.

$$J_E \cong \lambda(T_a) \sum_{i=1}^{i=n} \frac{\Delta \rho v,i}{\Delta t} \Delta z_i \qquad (11)$$

The vegetation storage ($J_S$) was reduced to just stem storage of the measured Norway spruce as noted by Equation (12). Wet biomass was denoted by $m_{veg}$, and $c_{veg}$ refers to the specific heat of the given vegetation, in this case Norway spruce. Change in temperature ($\Delta T_{veg}$) was recorded from probes placed in a profile up the stem of four trees and averaged.

$$Js = m_{veg} c_{veg} \times \frac{\Delta Tveg}{\Delta t} \qquad (12)$$

Lastly, the biochemical heat storage, $J_c$, in Equation (13), was calculated. Here μ represents the specific energy for photosynthetic activity ($10.88 \times 10^6$ J/kg $CO_2$) and GPP is gross primary production.

$$J_c = -\mu \times GPP \qquad (13)$$

All of these used the thirty-minute continuous data mentioned previously from ICOS Sweden Carbon Portal (2018). For a more in-depth look at the original equations in addition to the biochemical heat storage, please look to (Moderow et al. 2009) where both the original and simplified equations are available. Measurement data units for energy balance equations, as well as, water and carbon balance units can be found in Table B of the appendix.

*3.3.3 Closing the Energy Balance*

After total storage was calculated for the entire study period the energy balance was reevaluated to see how close it was to complete closure. This was done by looking at the energy balance ratio, EBR, (Equations14a & 14b) as well as comparing the finalized available energy to the turbulent fluxes one last time. Aside from the whole study period, EBR was also defined at different temporal scales for pre and post-correction and under differing atmospheric conditions for pre-correction to determine when the energy balance was closest to complete closure and inversely when issues with energy closure occurred.

$$EBR = \frac{\Sigma(H+LE)}{\Sigma(Rn-G)} \qquad (14a)$$

$$EBR = \frac{\Sigma(H+LE)}{\Sigma(Rn-(G+G_S)-J)} \qquad (14b)$$

The Bowen ratios, β, (Equation 15) and the evaporative fractions, EF, (Equation 16) were also obtained to get a better idea of where energy was moving through the system during the study period, specifically with regard to the turbulent fluxes, sensible and latent heat. From these metrics, one can see which flux was greater at any given time throughout the spring through fall seasons.

$$\beta = \frac{H}{LE} \qquad (15)$$

This was to illustrate which of these two fluxes were contributing most to the energy balance at any given point in time during the study period, aside from winter months, when latent heat is too low to produce meaningful Bowen ratios or evaporative fractions.

$$EF = \frac{LE}{H+LE} \qquad (16)$$

Diurnal patterns for all energy components were defined by hourly means to observe trends. These also served as an indication for how energy behaved in this specific environment in order to better understand the other underlying processes at play.

## 3.4 Hydrological Components

In addition to energy components, the primary hydrological components of the water balance were quantified to see where water moved through the forest at given points in time throughout the study period. There was a drought that occurred throughout 2016 that placed a lot of supplementary stress on the local environment, including the vegetation and soil water. This meant that outcomes between the study years varied quite substantially. This can be seen in the results represented by the water balance and the separate hydrological components that constitute this balance. For the scope of this study, the water balance was kept quite simple while still ensuring the main components were accounted for.

### *3.4.1 Water Fluxes and the Water Balance*

A four-variable Equation (17) was chosen for the water balance. Three of the four variables: precipitation (P), actual evapotranspiration (ET), and change in soil water storage ($\Delta S_w$) were readily determined from ecological data available on the ICOS Carbon Portal. For water storage (Equation 17) specifically, only soil water content was used since ground water measurements were not taken until mid-July of 2015. For consistency sake it was decided that this was the best solution. Nevertheless, the groundwater data that was available was used to calculate changes in groundwater storage. This was observed separately from soil water storage. The last variable: discharge (Q) was the subsequent remaining water in the system to close the water balance. Error ($\eta$) was added to discharge to signify this assumption of incomplete water balance closure (Jones et al. 2017).

$$P = ET + \Delta S_w + Q + \eta \quad (17)$$

This was inspected at different temporal resolutions, though scales no shorter than a day were included results due to issues with graphical readability at finer temporal scales. In general, it is assumed that change in water storage can often be neglected because these changes remain so small. However, when it was examined at a finer temporal scale, this certainly did not appear to be the case. Furthermore, because the 2016 drought had an impact on the normal distribution of water in the forest, the typical expectations for water storage varied from this norm. Because of this, it was incredibly important to include soil water storage in the water balance analysis. If it had been neglected, these gradations would have been missed. The change in the water storage within the soil profile was calculated using volumetric water content ($\Theta$) measurements at different levels (z) within the soil column (Equation 18) based on (Almeida et al. 2007).

$$[\sum_{i=1}^{n} \Theta_i \, z_i]_{final} - [\sum_{i=1}^{n} \Theta_i \, z_i]_{initial} \quad (18)$$

Actual evapotranspiration for the system was calculated using the temperature dependent latent heat of vaporization ($\lambda$) and latent heat turbulent fluxes (LE) seen in Equation 19 below. This was used both in the water balance and the water use efficiency analysis.

$$\frac{LE}{\lambda} = ET \quad (19)$$

## 3.5 Carbon and Ecosystem Exchanges

As with the water cycle, the cycling of carbon through the forest is largely interconnected with both the water and energy cycles (Beer et al. 2007). To dissect this interconnectivity, the movement of carbon in the forest was examined. This took the form of gross primary production (GPP), net primary production (NEP), and ecosystem respiration ($R_{eco}$) at the ecosystem level (Equation 20). The 30-minutes values for GPP and $R_{eco}$ were derived from flux partitioning of Net Ecosystem Exchange (NEE) measurements using the method outlined by (Wutzler et al. 2018). Net NEE

was changed to NEP for this study. These values were converted from μmol C $m^{-2}$ $s^{-1}$ to grams C $m^{-2}$ $s^{-1}$. Similarly, fluxes of $CO_2$ were converted from μmol $CO_2$ $m^{-2}$ $s^{-1}$ to grams $CO_2$ $m^{-2}$ $s^{-1}$

$$NEP = GPP\text{-}R_{eco} \qquad (20)$$

Gross primary production, often used as a general proxy for preliminary ecosystem productivity, also serves as a good indicator for environmental stressors such as water shortage when initial productivity drops below typical norms (Zhang et al. 2016). This was inspected at the monthly level to get a better idea of how deviations in the energy and water balance affected the productivity of vegetation.

### *3.5.1 Primary Production and Photosynthesis*

As expressed in Equation (20), net primary production can be calculated from the difference between gross primary production and ecosystem respiration. This essentially is a tell for how big of a carbon sink a forest, or any ecosystem for that matter, is at a given point in time (Gower et al. 1997). These relationships were also studied to see how carbon moved through this environment during the study period.

### *3.5.2 WUE from Evapotranspiration*

Inherent water use efficiency for a given ecosystem is easily obtained by looking at the relationship between chemical energy asbiomass, or production of useful chemical energy, and evapotranspiration. Equation (21) shows the simplified metric for achieving a basic understanding of the efficacy of the vegetation to sequester carbon for growth of vegetal mass (Kwon et al. 2018). Values of GPP were converted from μmol C $m^{-2}$ $s^{-1}$ to grams C $m^{-2}$ $s^{-1}$ and ET was expressed as kilograms $H_2O$ $m^{-2}$ $s^{-1}$.

$$WUE=\frac{GPP}{ET} \qquad (21)$$

When water use efficiency is high, it means that the given vegetation is efficiently producing biomass with minimal excess transpiration. On the contrary, when this metric is low, it is either an indication of low growth rate, possibly during the non-growing season, or an environmental stressor leading to higher than usual levels of transpiration, or quite often both. This was evaluated by looking at patterns in daily rhythms, as well as, seasonal cycles in WUE to see where the efficiency in vegetal carbon metabolism lie.

# 4 RESULTS

As expected, the fundamental connections between the three cycles were described. Both system shortcomings and moments of high efficiency and growth were defined. Here we see how the drought and record temperatures worked against traditional norms for the study site. Conversely, we see where the things ran well, and the cycles ran smoothly.

Table 2. Land classification of five classes within the FFP (2D) by contour area starting from the closest area to the furthest.

| | Class 1 | Class 2 | Class 3 | Class 4 | Class 5 |
|---|---|---|---|---|---|
| Contour Area | Mixed Deciduous Forest | Roads, Built-up area | Semi-Natural Grass | Bare-soil and Cropland | Coniferous Spruce Forest |
| 10% | 0.28 | 0 | 0 | 0.023 | 0.697 |
| 20% | 0.248 | 0 | 0.003 | 0.049 | 0.7 |
| 30% | 0.257 | 0 | 0.003 | 0.058 | 0.681 |
| 40% | 0.255 | 0 | 0.004 | 0.069 | 0.671 |
| 50% | 0.275 | 0.001 | 0.005 | 0.068 | 0.652 |
| 60% | 0.289 | 0.001 | 0.005 | 0.061 | 0.644 |
| 70% | 0.292 | 0.001 | 0.004 | 0.059 | 0.644 |
| 80% | 0.288 | 0.001 | 0.004 | 0.059 | 0.65 |
| 90% | 0.287 | 0.001 | 0.004 | 0.062 | 0.646 |

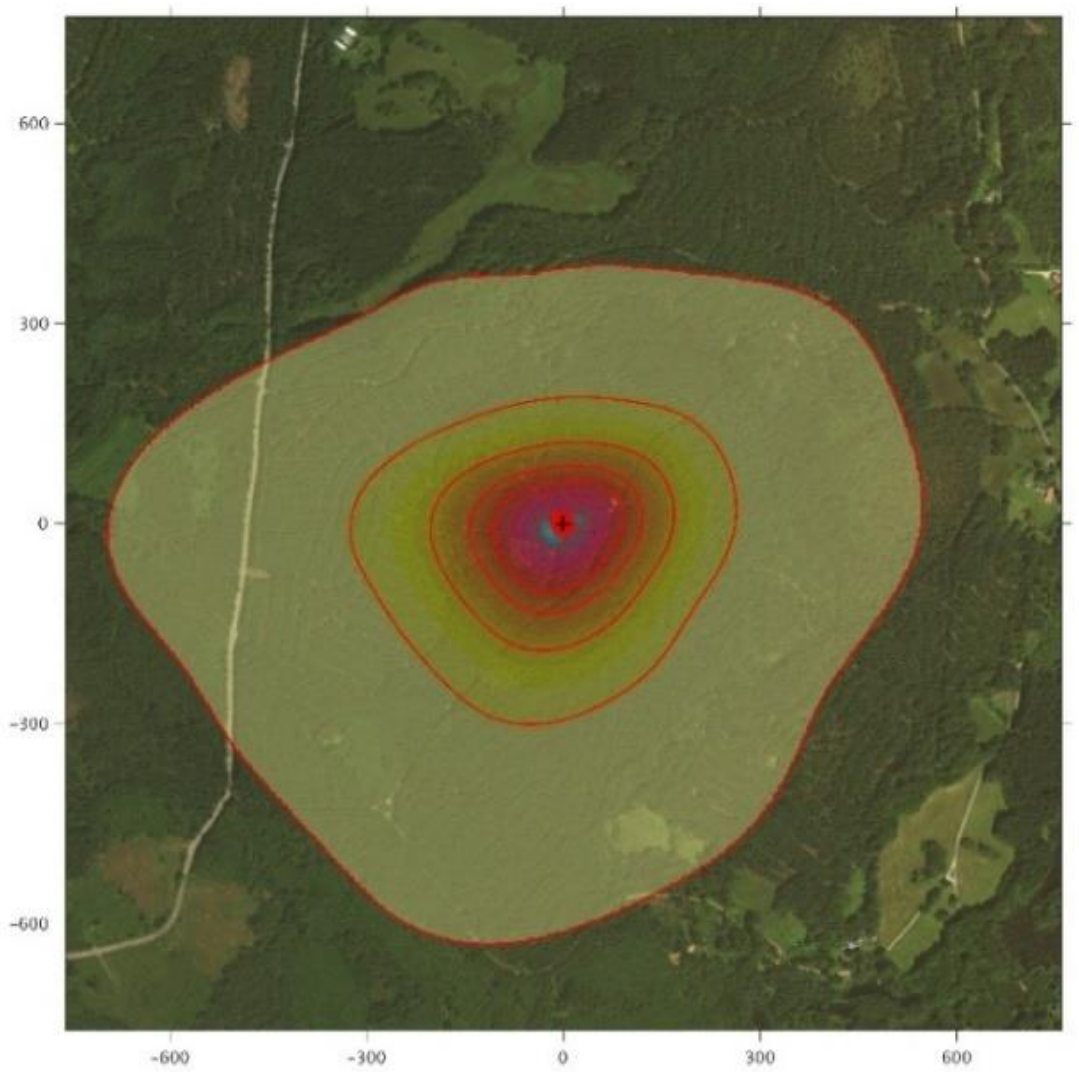


Figure 2. Flux Footprint Prediction (FFP 2D) for the entire study period from January 1, 2015 to December 31, 2016 using Kljun et al. (2015) model. Each contour line adds ten percent contribution to the flux density starting from the tower (red dot) at a measurement height of 27 meters. Axis marks in meters.

## 4.1 Site Conditions

Flux footprint analysis using the flux footprint prediction (FFP) online data processing tool indicated a high likelihood for accurate measurements of forest fluxes (Figure 2). Within the contour lines, majority of the data collected was measured from the canopy surface. Low instances of fluxes from non-desired landcover types were seen (Figure 3). If this had not been the case, then later assumptions made in this study would be rather precarious, since measurements could have been attributed to non-forested areas.

A look at Table 2 gives a better hierarchal classification of the likely source for the subsequent findings of this study. From here it is noted that a large majority of the footprint area was assigned to coniferous and deciduous forested classes, which was the main goal of the station investigators. Moreover, a visual of what that classification looks like can be seen in Figure 3. With surface roughness, displacement height, the wind characteristics, and several other atmospheric conditions taken into account, this predictive model visually outlines where the land source of the observational measurements were obtained.

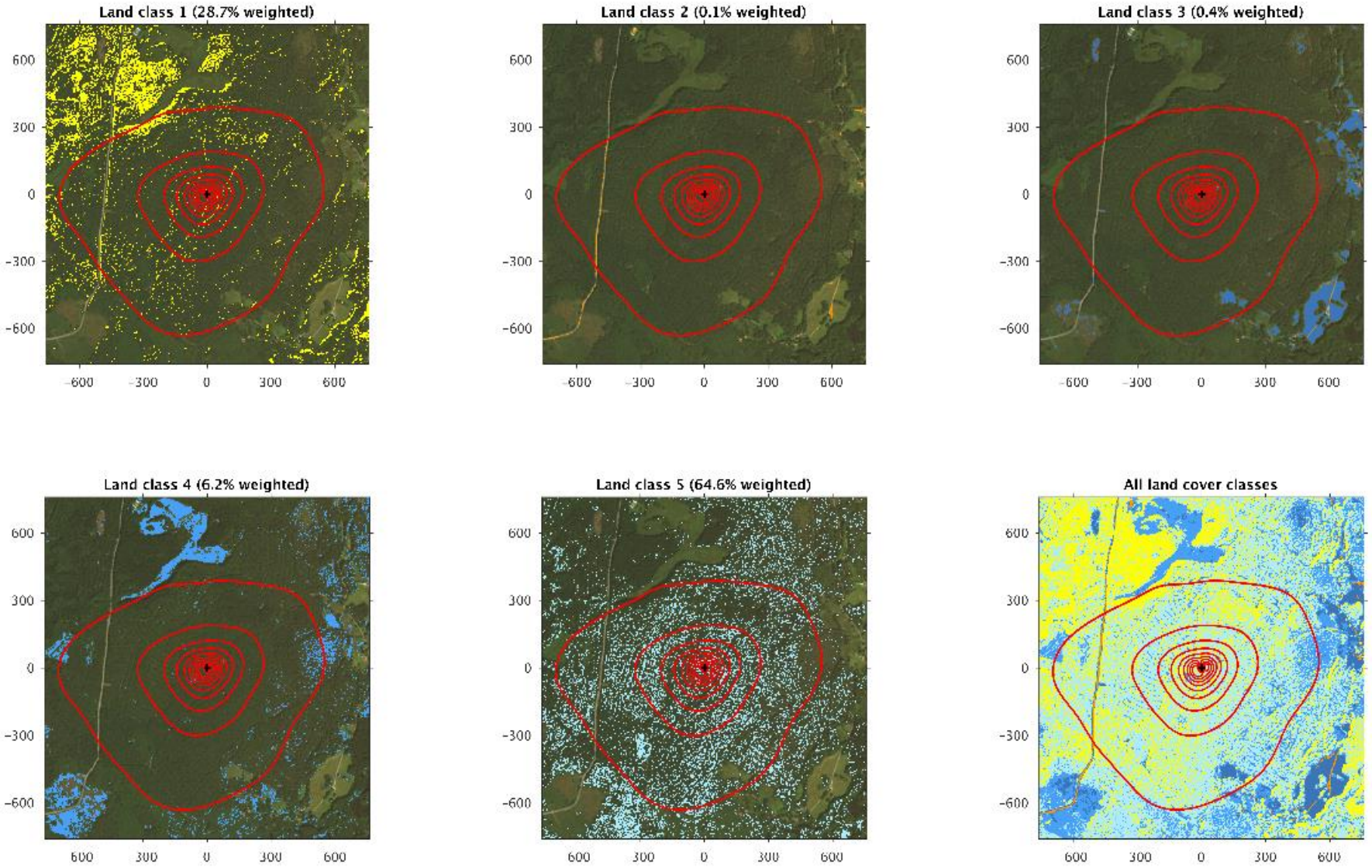


Figure 3. Classification of FFP 2D (Kljun et al., 2015) shows deciduous forest and coniferous forest (class 1 & 5) comprising ~93% of landcover. Other classes shown include roads, fields, and grass making up the difference. All five classes are shown together in the bottom right figure for reference.

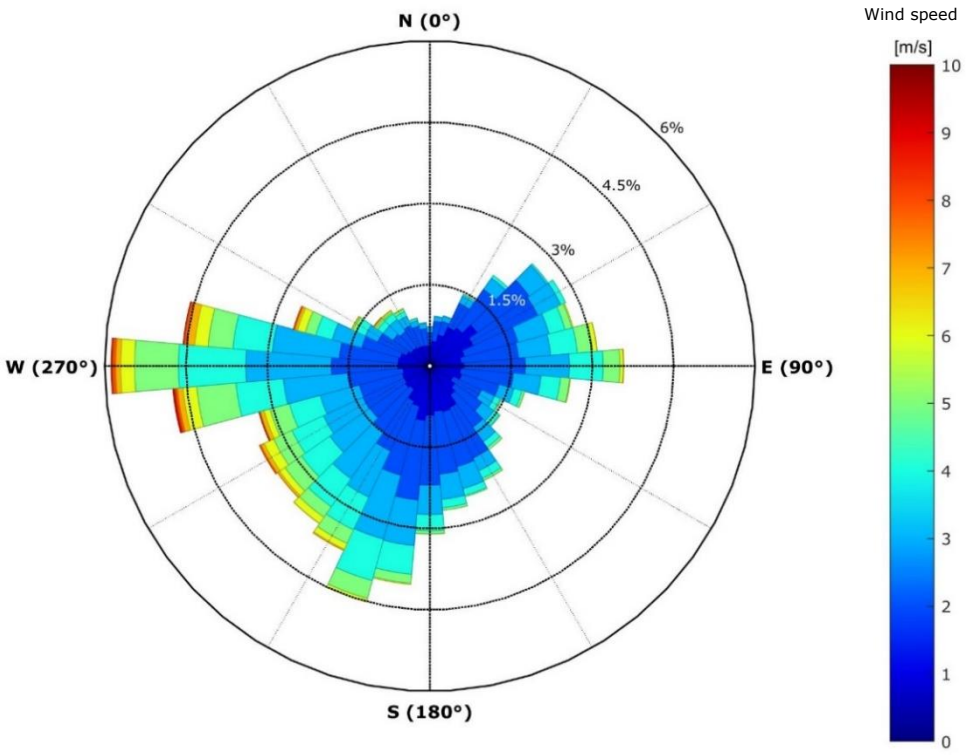


Figure 4. Windrose showing frequency of wind direction in degrees with wind speed in meters per second for the entire study period.

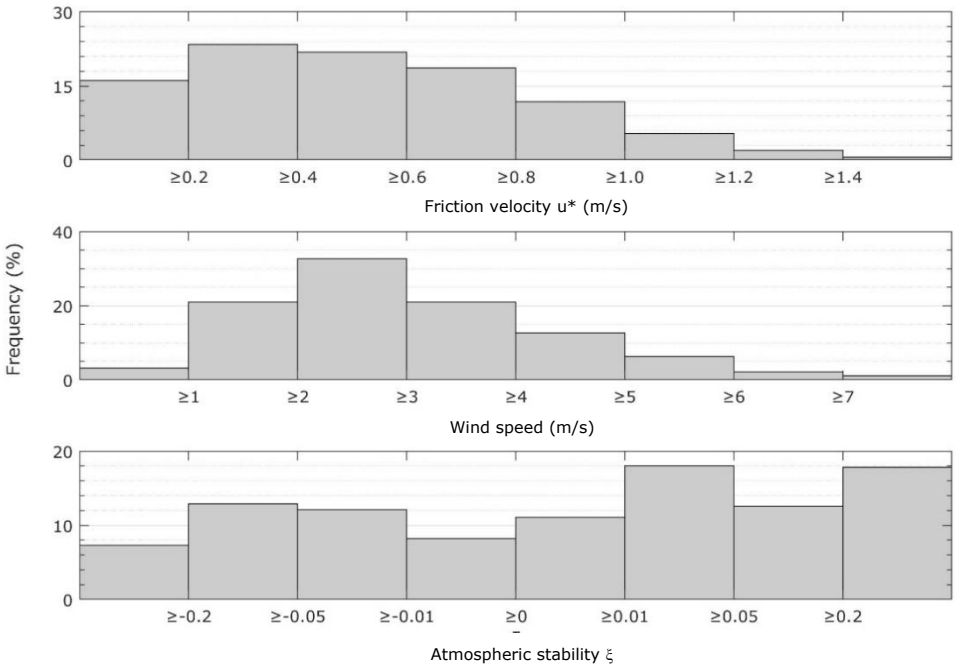


Figure 5. Histogram distribution of friction velocity (u*), wind speed frequencies, and atmospheric stability in frequency percentages for the entire study period.

This is a quantitative way to determine whether measurements are derived from the preferred or non-preferred landcover classes at the study site. To further understand the implications of these footprint findings look to (Kljun et al. 2015) model where the physical mechanisms of the aerodynamic and atmospheric conditions are better explained.

Windspeed and wind-direction for the study period are visualized in Figure 4. The predominant wind direction appears to be Westerly, followed by Southwesterly, and then Northeasterly. Top windspeeds were almost exclusively from the West, while speeds closest to zero tended to come more from the Northeast than the other quadrants. Frequencies of friction velocity, or shear velocity (u*), windspeeds, and the atmospheric stability (ξ) are allotted in Figure 5. The most dominant values for u* fell between 0.2 to 0.4 and went as high as 1.9 in a few instances, though more than fifty percent of measured u* was 0.8 or less. The most frequent windspeeds were between 2 and 3 m/s. Less than five percent of measured windspeeds were above 6 m/s. Atmospheric stability tended to fall within 0.01 to 0.05 or above 0.2. Both of which made up nearly twenty percent frequency each. Stability rarely dropped below -0.2 with less than seven percent frequency occurring for stability conditions less than -0.2.

It is also noted that there was a variation in albedo with relation to snow depth (Figure 6) during the study period. Aside from the obvious effects of local atmospheric cooling, this also serves as a good tool for looking at standard nature of forest radiation in the growing season. Because the site is hemiboreal in nature, less annual snow means shorter periods of albedo reflectance, and thus shorter periods of cooling negative feedbacks (Ponton et al. 2006) than boreal geographical locations. This is made evident when albedo falls below 0.1 from March to September for both study years as seen in Figure 6 (Liu et al. 2008). In addition, it is also apparent that peak snow depth was during December of 2015 and January of 2016. Other than that, average monthly snow depth remained below 0.06 meters for the other winter months during the study period. Snow present was likely compacted and denser than snow found at higher, more northern latitudes. These higher observed albedos seen in the winter months are also further supported by lower sun angles in the winter in higher latitudes far removed from the equator. These lower angles also contribute to higher reflectance of incoming solar radiation during these times. Inversely, during the summer and/or growing seasons, higher sun angles help to lower albedo eventually decreasing surface reflectance of incoming solar radiation (Coakley 2003).

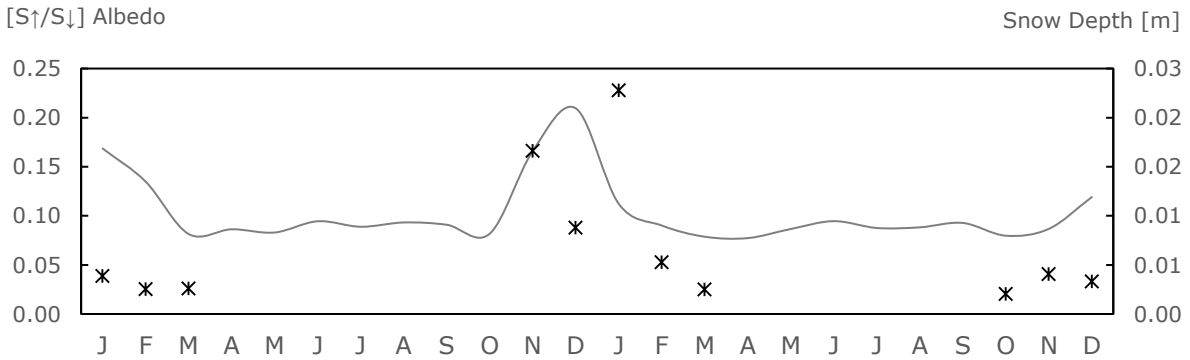


Figure 6. Midday (12:00 local standard time) reflectance of shortwave radiation, or albedo, (gray line) with growing season averages of about 0.08 and large fluctuation in albedo during non-growing season partially dependent on snow reflectance represented by average depth in meters (black points).

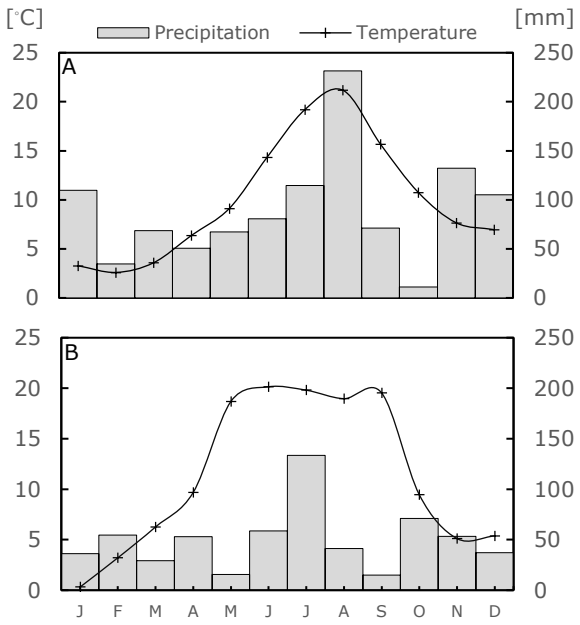


Figure 7. Monthly totals of precipitation in millimeters for 2015 (7A) and 2016 (7B) (gray bars), and monthly averages of temperature for 2015 (7A) and 2016 (7B) in degrees Celsius (black line with cross marks).

It can also be noted that monthly temperatures showed higher averages during the 2016 where averages plateaued from April all the way to September at around 20 degrees Celsius (Figure 7). For 2015 temperature seemed to follow a bell shape with relative lows progressing from January until they peak in August. From there they dip back down into the winter months. In general temperature often fell below 5 degrees Celsius well into April for both study years. With that said, this occurred more often in 2015 than in 2016. Nightly temperature lows into the spring showed unexpected dips followed by light snow. While mean temperatures never got exceptionally low, periodic events of temperature dips were not uncommon for the early spring when looking at the 30-minute temperature averages. In general, the climate during the study period was neither boreal nor

nemoral in nature, but rather a unique combination of the two. This is especially apparent when looking at fall temperature means where decreases in temperature appear to be delayed for both 2016, and especially 2015. Precipitation averages contrasted to monthly temperature means show generally low sums for precipitation for the drought year of 2016. This deviation coupled with the higher spring through summer temperatures made carbon, water, and energy cycling analysis all the more interesting. The opposite was true for August of 2015 where both temperature and precipitation hit annual highs for the year. As a whole 2015 experienced higher, on

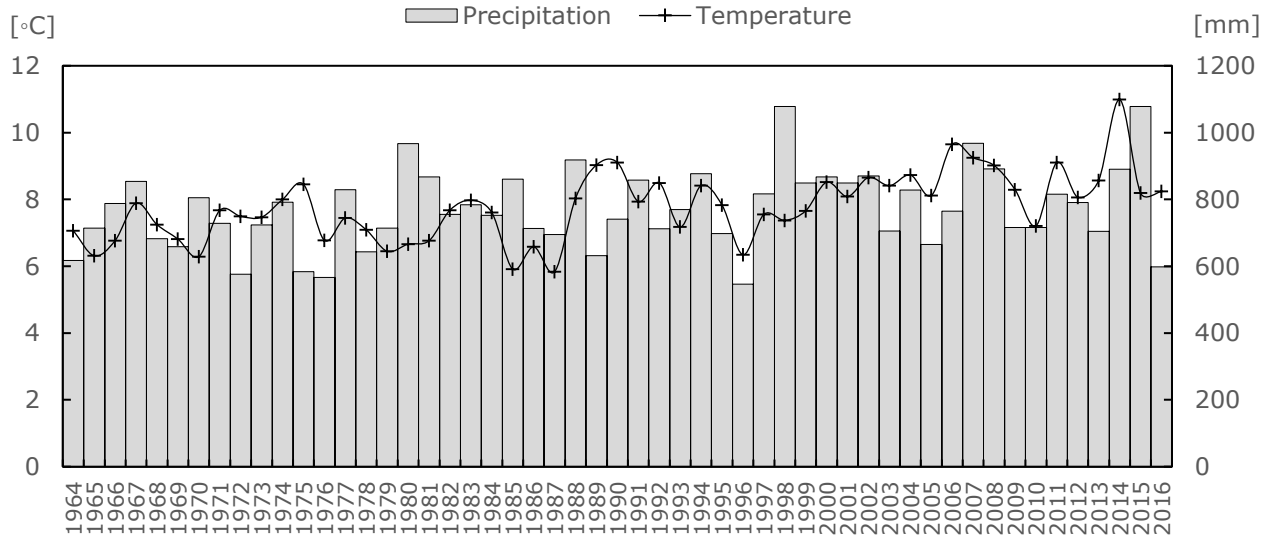


Figure 8. Annual totals of precipitation in millimeters (gray bars) for 50 years prior to study period calculated from SMHI data followed by the two-year study period calculated from ICOS Hyltemossa data, and annual averages of temperature in degrees Celsius (black line) for 50 years prior to study period calculated from SMHI data followed by the two-year study period calculated from ICOS Hyltemossa data.

average, monthly precipitation sums, with the exception of October of that year. Figure 8 shows how average annual temperature and total annual precipitation during the study years compared with the previous fifty years.

Relative humidity, and especially vapor pressure deficit, were evaluated on a smaller temporal scale for modeling some of the energy balance components. Daily averages starting after mid-May of 2015 for relative humidity vapor pressure deficit are shown in Figure 9. Unfortunately, relative humidity, like the specific humidity profile, was not recorded until the middle of 2015. However, both years at first glance appear to follow a relatively similar pattern with July to September of 2015 and 2016 ranging mostly between 0.5 and 1.0 kPa. The winter months inversely exhibit site lows for vapor pressure and highs for average relative humidity occurring during these months. On average, this site, as predicted by global climate models, seems to be quite humid. While observed values of relative humidity in winter appears to hold more moisture in the air, spring and summer months still show quite high moisture retention at about 70-80% relative humidity. It would be interesting to see if spring of 2015 had followed similar incline as 2016, where humidity appeared to drop and vapor pressure appeared to peak. With 2015 quite a bit more precipitation, one could assume that the air moisture for this year was higher on average.

Daytime solar radiation, shown at the top of Figure 9, reached daily averaged peaks nearly as high as 400 W $m^{-2}$ during the summer, growing seasons. For the winter months, averaged daily solar radiation was often below zero. Photosynthetically active radiation (PAR), in μmol $m^{-2}$, followed a very similar pattern to solar radiation, as also depicted at the top of Figure 9. PAR shows seasonal curves that are relatively similar for both years. Peak average daily PAR started as early as May in 2016, while 2015 PAR did not peak until July. This is a great early indication for how other radiative patterns would be for the study period, since net radiation seemed to have a similar pattern as PAR, which makes sense since these variables are quite related to one-another These implications for overall light conditions during the study period also serve as an indication for how carbon cycling will perform in relation to growth in biomass, should other environmental stressors like water shortage or invasive pest stress be low. It can also be noted that on average, PAR seemed to be lower for 2015 and in 2016, and ideal light conditions seen starting around April into September for both study years.

Daily totals of precipitation (mm) and fluctuations in averaged daily volumetric soil water content (%), as seen in Figure 9, provide a mild window into what the overall water balance for the study site will look like. In Figure 7, the lows of total precipitation in 2016, as apposed to the previous year, are more apparent on the monthly level. On a daily scale it is slightly harder to discern the less frequent events of precipitation. Volumetric soil water content (SWC %) was highest in the winter months to early-spring for 2015 and mid-spring for 2016 with content being on average well over thirty percent. Soil water content began to fall below a daily average of thirty percent during the growing season from spring 2015 to fall in 2015 and all the way into December in 2016. More instances of soil water content falling below twenty percent occurred in 2016, largely due to the drought that occurred that year at this forest site when incoming water in the form of precipitation was lower. Daily average air and canopy temperatures (Figure 9) were almost virtually the same with similar temporal patterns, yet canopy temperature was always marginally lower than air temperature. Lows for both occurred in the winter months, and increased in the spring, peaked in summer, and started their descent again in the fall with the hottest temperature happening in June of

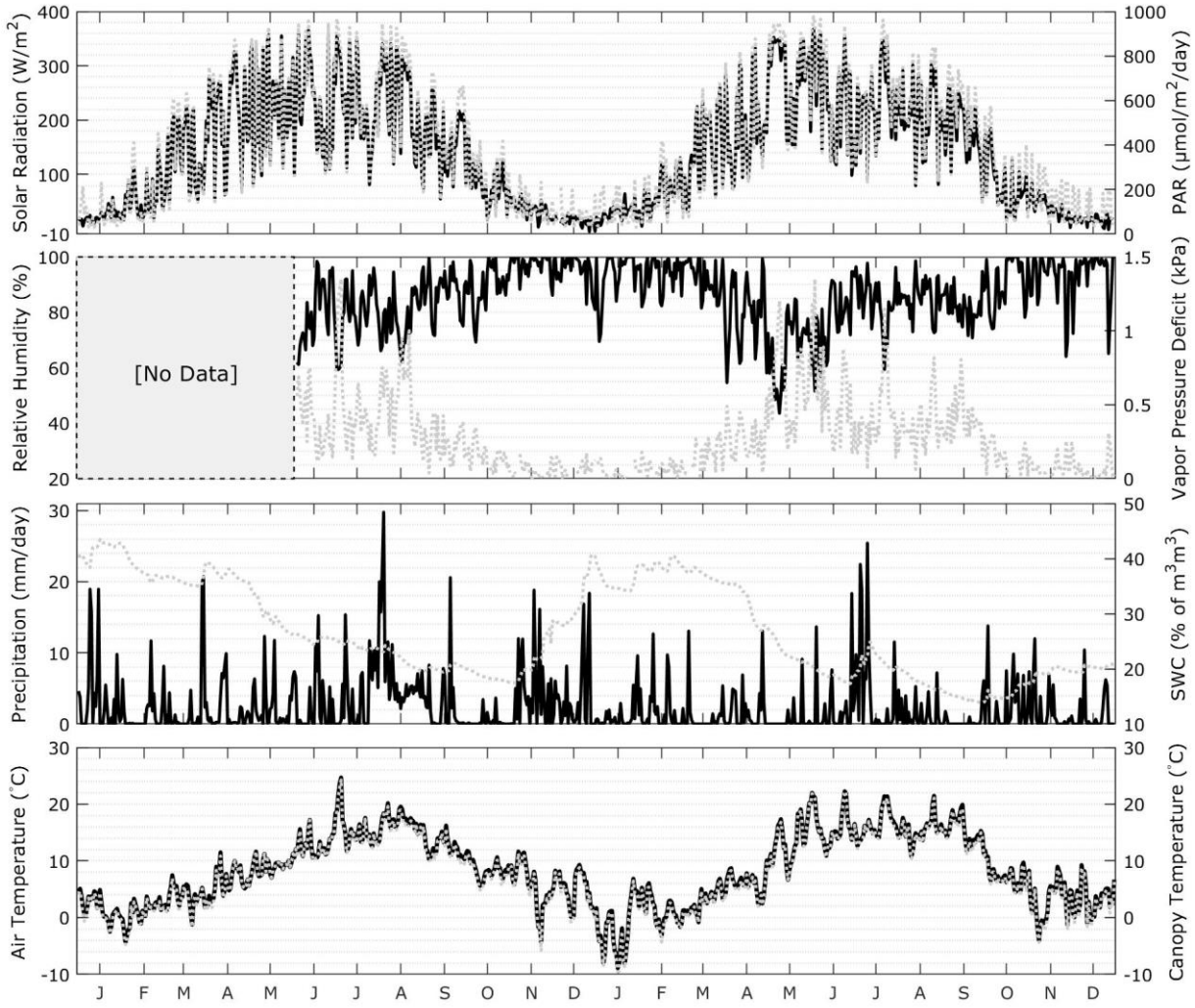


Figure 9. Daily averages of daytime (global radiation >10 W $m^{-2}$) solar radiation (W $m^{-2}$) and daytime photosynthetically active radiation (µmol m-2 s-1), daily averaged of relative humidity (%) and vapor pressure deficit (kPa), daily total precipitation (mm $day^{-1}$) and average volumetric water content (%), and daily average air temperature (◦C) and average canopy temperature (◦C) with first y-axis variables in black and second y-axis variables in light gray.

2015 and lowest temperature occuring in Janurary of 2016. The variances of temperature can best be seen on the monthly scale (Figure 7) where the summer months between the years somewhat differ.

## 4.2 Energy Balance

Several parts of the energy balance were explored in detail for the purpose of this study, where we see the outcomes of modeled energy balance results along with the quality of data used. Both of which proved to have quite favorable results.

### *4.2.1 Energy Balance Closure*

The net radiation to short and longwave flux regression showed a slope of 1.0, an intercept of -1.08 $Wm^{-2}$, and an $r^2$ of 0.99 indicating a near perfect relationship between the measured net radiation and the sum of the individual long and shortwave radiative measurements.

The initial evaluation of the energy balance closure before gap-filling was strong (Table 2, Figure 10a). The $r^2$ shows a high correlation between the two variables at

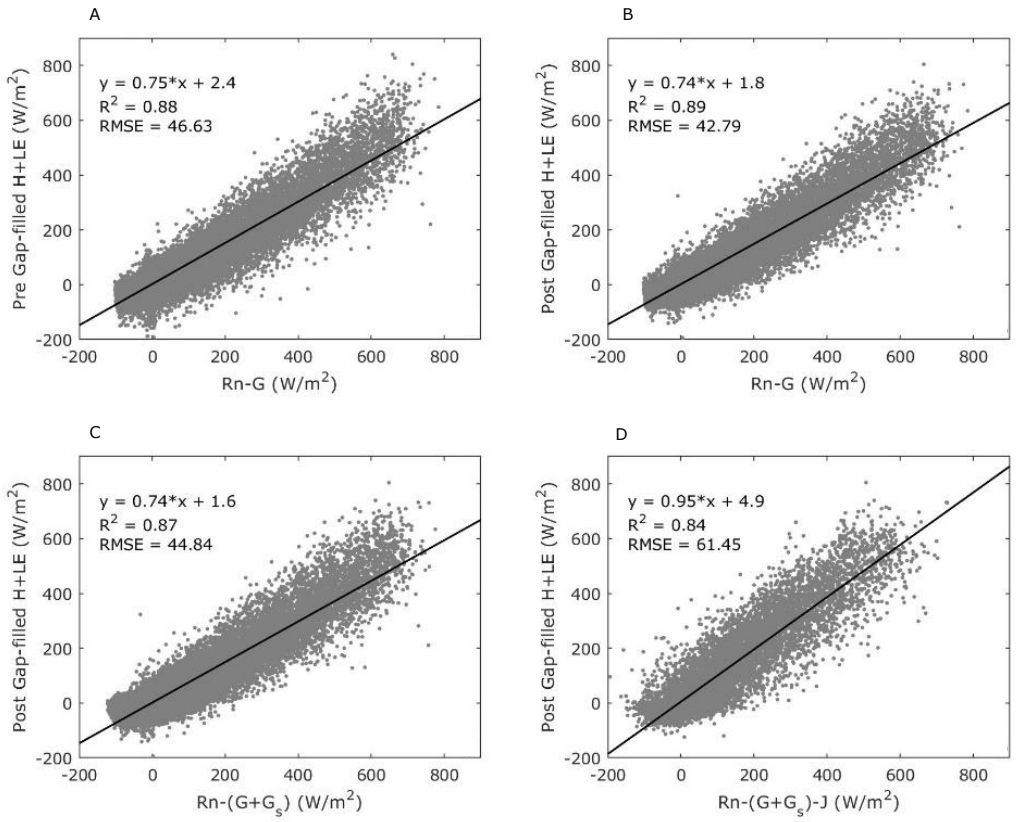


Figure 10. Energy balance closure represented by the slope with $r^2$ and RMSE values included for a) net radiation minus uncorrected ground heat flux (x-axis) versus sensible heat plus latent heat before gap-fill (y-axis) b) net radiation minus uncorrected ground heat flux (x-axis) versus sensible heat plus latent heat after gap-fill (y-axis) c) net radiation minus corrected ground heat flux (x-axis) versus sensible heat plus latent heat after gap-fill (y-axis), and d) net radiation minus corrected ground heat flux and storage (x-axis) versus sensible heat plus latent heat after gap-fill (y-axis).

0.88. The RMSE also remained somewhat low indicating a decent start. However, the slope between turbulent fluxes and available energy and the EBR were both 0.75 indicating 25% of unexplained difference in available and turbulent fluxes.

After gap-filling (Figure 10b) and gap-filling plus soil heat flux correction (Figure 10c) the slopes decrease and the EBRs slightly increase, indicating a problem still in energy balance closure. The y-axis intercepts do decrease both of these, and $r^2$ values remain quite high with the highest seen during the post gap-fill, pre-soil heat flux correction comparison. Once calculated storage was taken into account the $r^2$ value decreased and the RMSE increased indicating a slightly weaker correlative relationship (Figure 10d). This is apparent with the EBR and slope improvement by about 0.26 0.20, respectively. This was by far the closest any of the four energy balance slopes got to achieving complete energy balance closure, though EBR was overestimated by 0.013 following storage correction. This shows that while storage predictions may have been periodically overexaggerated, as a whole,

Table 3. Energy balance closure statistics over the course of the correction process starting with initial values before gap-fill, followed by values after gap-fill, surface heat flux correction (G), and surface heat flux and modeled storage (J) corrections.

| | $r^2$ | Slope | Offset (W $m^{-2}$) | RMSE | EBR |
|---|---|---|---|---|---|
| Before Gap-fill | 0.88 | 0.75 | 2.4 | 46.63 | 0.750 |
| After Gap-fill | 0.89 | 0.74 | 1.8 | 42.79 | 0.766 |
| After GF, G Correction. | 0.87 | 0.74 | 1.6 | 44.84 | 0.769 |
| After GF,G & J Corr. | 0.84 | 0.95 | 4.9 | 61.45 | 1.013 |

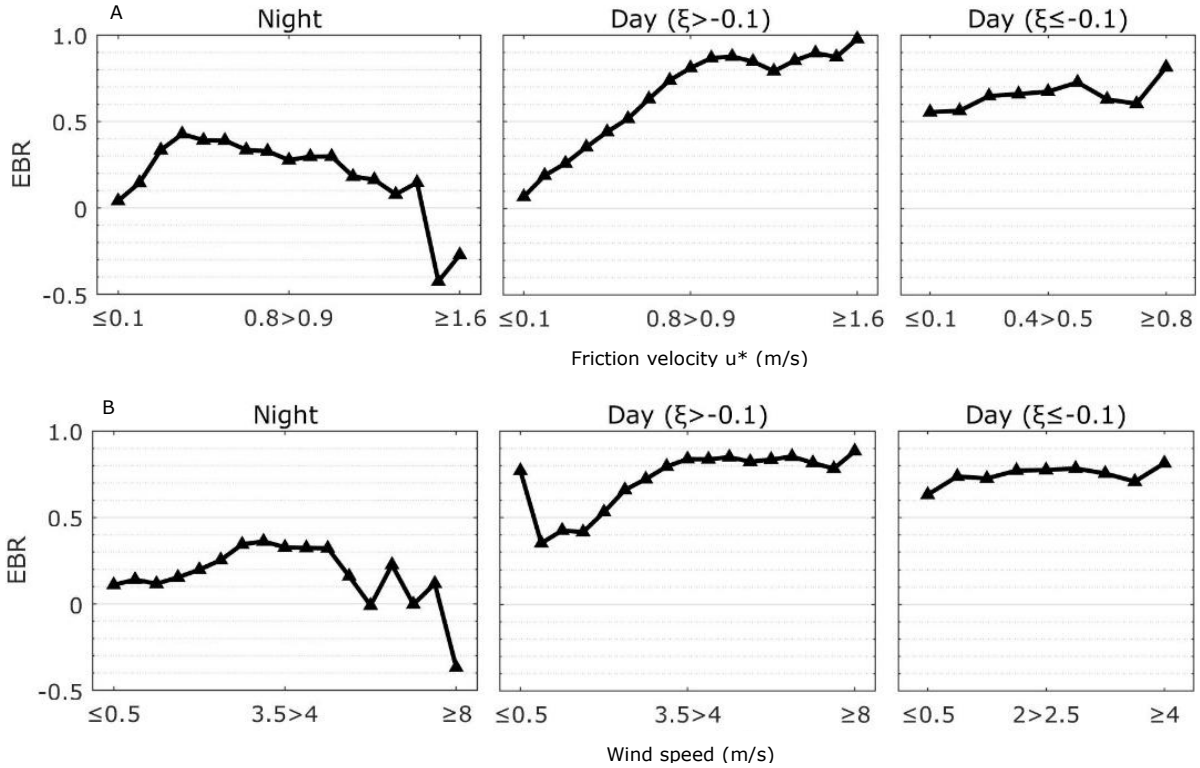


Figure 11. Energy balance ratios (EBR) for nighttime (global radiation < the 10 W $m^{-2}$), daytime stable and neutral (ξ>-0.1), and daytime unstable (ξ≤-0.1) versus friction velocity (m $s^{-1}$) in 11A and windspeed (m $s^{-1}$) in 11B.

they proved the best for reducing the sizeable gap in the energy balance for these study conditions. Table 3 best illustrates the statistical progression of energy balance closure at each step in the correction process.

As Figure 11 indicates, energy balance ratios for the energy data prior to energy storage correction were greatly affected by the state of wind speed, friction velocity, atmospheric stability and the time of day. The EBRs were at their worst during the nighttime with the lowest EBRs occurring at higher windspeeds and friction velocities. Nighttime EBRs never reached higher than 0.5. Contrary to this, the EBRs were at their highest during stable and neutral atmospheric conditions (ξ>-0.1) when the windspeed and friction velocity (u*) were high. The EBRs well over eighty percent when u* was greater than 0.9 m $s^{-1}$ and windspeeds were greater than 3.5 m $s^{-1}$ during stable or neutral atmospheric conditions. Below these friction velocities and windspeeds, the EBRs were gradually lower with decreasing friction velocity and windspeed. During unstable atmospheric conditions (ξ≤-0.1) the EBRs stayed within sixty to eighty percent with the highest values, again, occurring at both the higher windspeeds and higher friction velocities conditions.

### *4.2.2 Diurnal Patterns of Radiation*

Average daily cycling trends for the individual energy components were explored to better comprehend their general nature throughout a typical year. Figure 12 provides a visual que to what these patterns look like. As expected, net radiation followed a bell-curve pattern with peaks around midday. Both ground heat flux and ground heat flux plus ground storage flux followed a similar pattern to one-another with a down curve during morning until midday when fluxes become positive. The magnitude of this is exaggerated in the ground heat flux plus ground storage flux, compared to the ground heat flux alone where the range goes from $\pm 1.0$ to $\pm 5.5$.

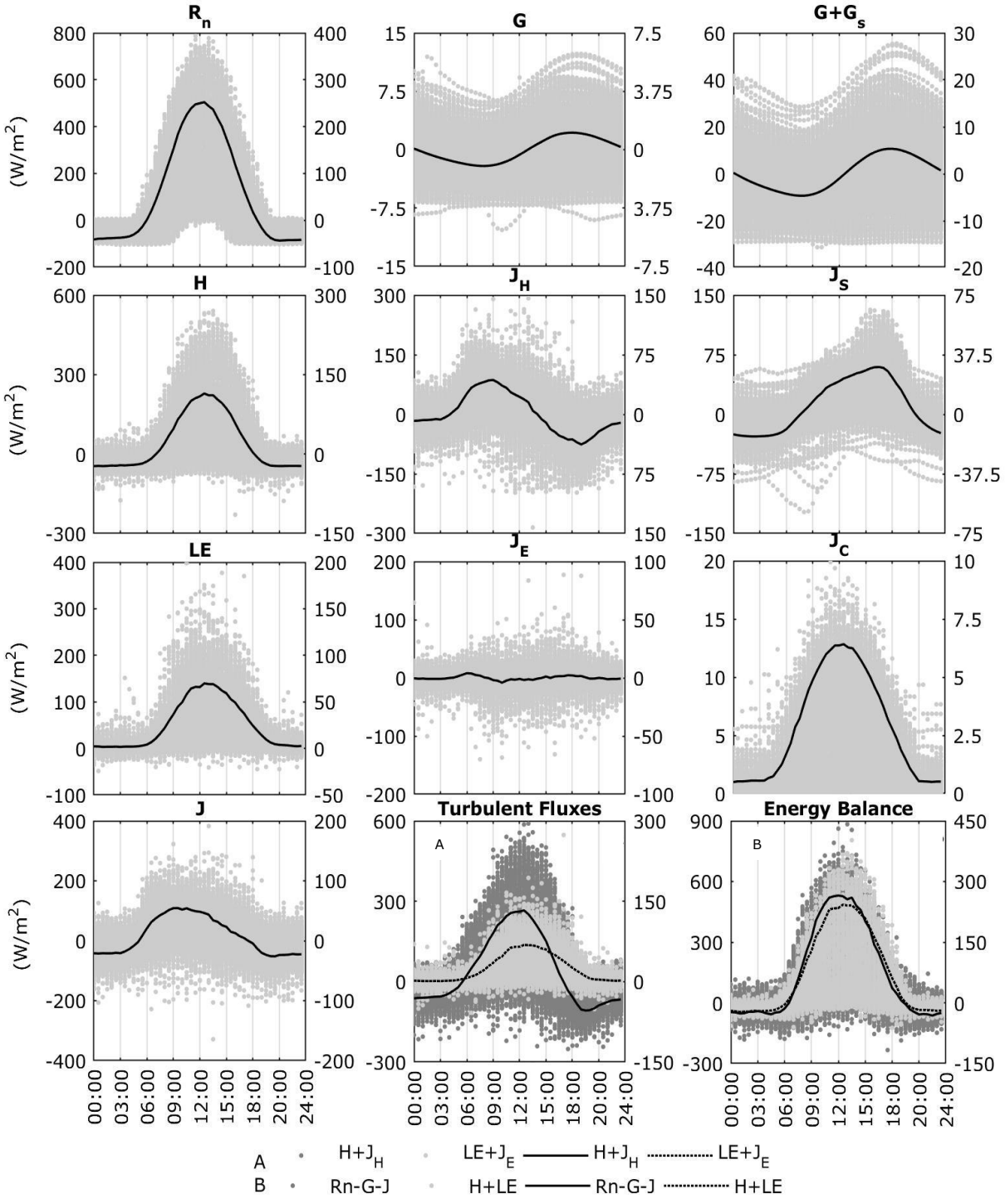


Figure 12. Diurnals patterns of radiation components in watts per square meter: Rn (net radiation), G (ground heat flux), G + Gs (ground heat flux and ground heat storage change), H (sensible heat flux), $J_H$ (sensible heat storage change), $J_S$ (stem heat storage change), LE (latent heat flux), $J_E$ (latent heat storage change), Jc (biochemical heat storage change), J (sum heat storage change), H+ $J_H$ (sensible heat flux and storage) and LE+ $J_E$ (latent heat flux and storage), Rn-G-J and H+LE. Black lines indicate averages for each component scaled on the second y-axis. The same is true for turbulent fluxes (12A) and energy balance (12B) except line and dot colors indicated by corresponding legend descriptions.

Sensible heat flux, latent heat flux, biochemical heat storage, and total storage follow a similar pattern to net radiation though on a much smaller scale since they only make up part of the net radiation, separately. The magnitude of these curves is biggest in the sensible heat flux, followed by latent heat flux and total storage. The

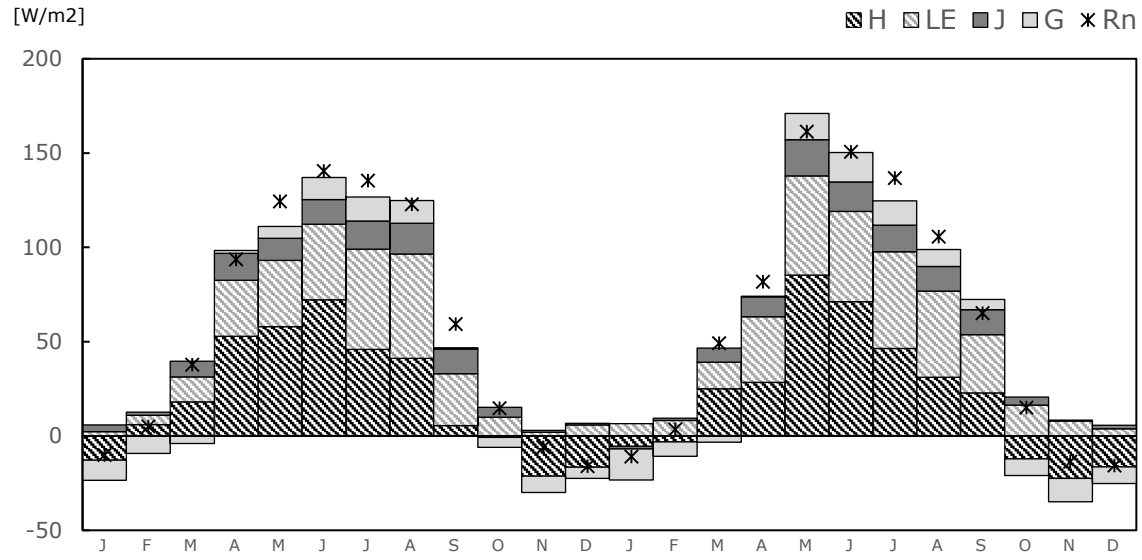


Figure 13. Monthly averages for the individual energy components after modeled energy correction: sensible heat (H), latent heat (LE), ground heat flux (G), and change in energy storage (J) compared to monthly averages of $R_n$ in W $m^{-2}$ for both study years side-by-side.

comparison of sensible to latent heat flux can be seen in the bottom of Figure 12. Here one sees an overall smaller peak in latent heat compare to sensible heat, as well as, a lag in the curve drop compared to the sensible heat flux. Sensible heat storage appears to have a much more exaggerated, but inverse pattern to the soil fluxes, while vegetation stem storage seems to have a lagged bell-curve, indicating a slight delay in energy transfer from storage. Here it can also be noted that the curve appears to be imperfect with a slight reduction in incline before ultimately peaking around dusk. This could be accredited to the insulating nature of the stems, and their ability to retain heat after surrounding air has cooled down. Lastly there is the latent heat storage that looks almost as if there is there is no real, observable pattern. This is largely in part to

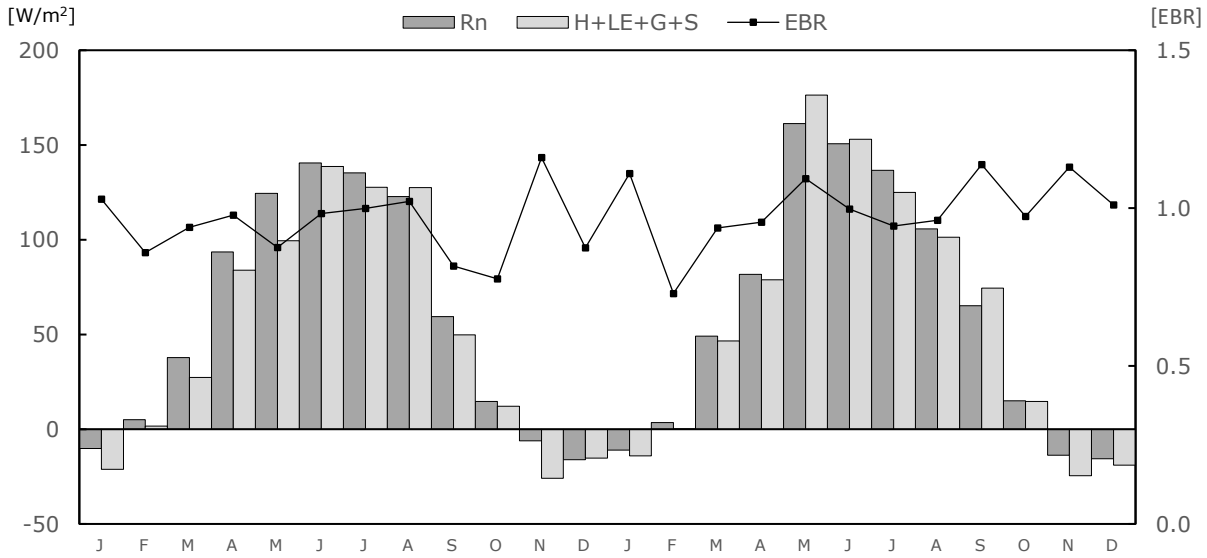


Figure 14. Net radiation and total remaining energy components (sensible heat, latent heat, ground heat flux, and energy storage). The energy balance ratio (EBR) can be seen on the right with its own secondary axis. This is to reference monthly energy balance performance where EBR = (H+LE)/(Rn-G-S).

its nearly exclusive dependence on the varying vapor characteristics of the forest air. These air column conditions fluctuate quite substantially throughout the day and certainly throughout the year.

A cumulative look at the diurnal patterns of the collective energy components can be seen in the bottom right corner of Figure 12 where the available energy curve ($R_n$-G-J) and the turbulent fluxes (H+LE) are placed side by side. The turbulent fluxes seem to only slightly undershoot the available energy arc during the midday hours from 11:00 to 15:00. Other than this minor incongruity, the daily pattern for available energy and the turbulent fluxes mirror each other quite closely.

*4.2.3 Temporal Energy Cycling*

Overall, there was harmony between net radiation and the sum of its parts for both study years. On a daily, and even monthly scales, it was obvious that sensible heat seemed to be the largest contributor within the forest energy balance (Figure 13). Naturally it was not surprising then that sensible heat storage also offered the most sizeable addition to the net energy storage throughout all seasons. The second largest contributor to net radiation was the turbulent latent heat flux. Latent heat fluxes were understandably larger in the summer months and decreased in the winter as they typically do in seasonal environments. However, storage from latent heat contributed far less to total energy storage. Last, and in this case least, ground heat fluxes and total storage change were both quite small when paralleled to the other parts of the energy balance.

This was especially apparent during the winter months when the extent of the collective storage fluxes decreases to nearly zero and the ground fluxes became negative on average. It is during these winter months were the greatest variance in energy balance closure ratio (EBR) can be seen (Figure 14). During the growing season, EBR stayed quite close to 1.0, and the EBR for the entire study period was 1.013.

Using the Bowen ratio (a) and evaporative fraction (b) for the grow season, the dynamic between the turbulent fluxes can be better explained (Figure 15). In April of 2016 and July of 2015 and 2016, the Bowen ratio reaches 1.0 indicating an equilibrium between sensible and latent heat fluxes. Typically, a Bowen ratio less than 1.0 is indicative of a surface with an abundance of water supply where a greater proportion of the surface energy is passed to the atmosphere as latent heat. The inverse is true

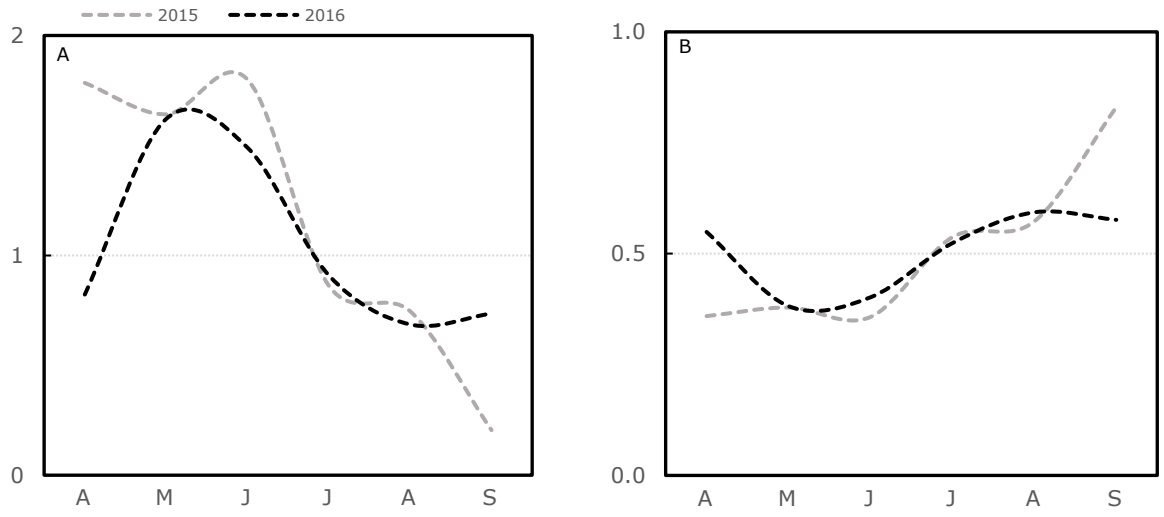


Figure 15. The 15A Bowen ratio (H/LE) and 15B evaporative fraction (LE/LE+H), during the growing season (from April to September), visually convey the relationship between sensible and latent heat fluxes.

for a ratio greater than 1.0 where more sensible heat is passed (Lewis 1995). Between April to July for both years the ratio is higher than 1.0 indicating larger sensible heat fluxes, and from July through September it drops below 1.0 indicating larger latent heat fluxes. The evaporative fraction signifies how much of the total turbulent fluxes can be accredited to latent heat. In July to September it appears that LE makes up more than half of the turbulent fluxes for both years according to evaporative fractions in those months. This is also the case for April of 2016. When evaporative fractions are higher than 0.5, this indicated that at more than half of the turbulent fluxes are latent heat.

## 4.3 Water Balance

Water cycling for the study period varied for all components accounted for. Here, the effects of the drought of 2016 on the water cycle become apparent when compared to the year prior, which had more precipitation and lower temperatures. When comparing the two study years with the average 50-year annual total precipitation of 765 mm, as presented in Table 1, it is apparent that 2015 was a rather abundant year with 1077.71 mm of total precipitation, while 2016 experienced an atypical shortage in incoming rainfall with only 598.36 mm of total precipitation. Table 4 best depicts the overall breakdown of the water balance components covered during the entire study period where differences between the years can be seen. The subtle and not so subtle fluctuations of the water balance components will be explained here by taking a finer look into their changing values over smaller, varying time scales.

### *4.3.1 Precipitation and Snow Water*

Precipitation for 2015 was nearly double that of 2016 as earlier depicted by monthly and daily illustrations. A cumulative look at precipitation (Figure 20) shows where this drop off in incoming water occurs. As with

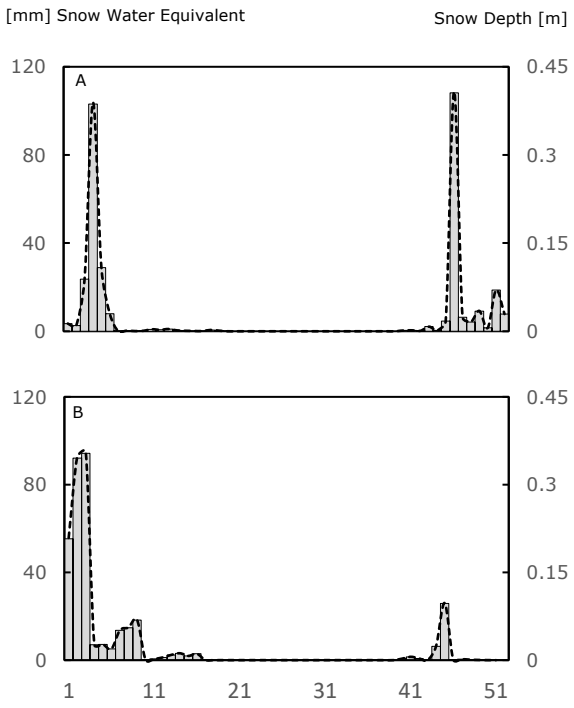


Figure 16. Total snow water equivalent (mm) in gray bars and average snow depth (m) in black dashed line for 2015 (16A) and 2016 (16B).

rainfall, a decrease in snowfall was also noteworthy especially for late 2016 when compared to the same months in 2015 (Figure 16). For early 2016 however, snowfall abundance is likened to that of the snow experienced in 2015. The cumulative drops in incoming water into the forest system had a domino effect on the remaining components of the water balance. Here we see an overall interruption in the typical behavior of the remaining components of the forest water balance.

### *4.3.2 Latent heat for Evapotranspiration*

A look at latent heat flux densities indicate a general pattern for forest evapotranspiration falling below 50 watts per square meter for winter months and early morning and evening hours. (Figure 17). Both years experienced similar sums in evapotranspiration with 2016 having slightly

higher values of ~360mm than 2015 at ~316mm (Figure 20). This could partially be explained by water stress from lower available soil water.

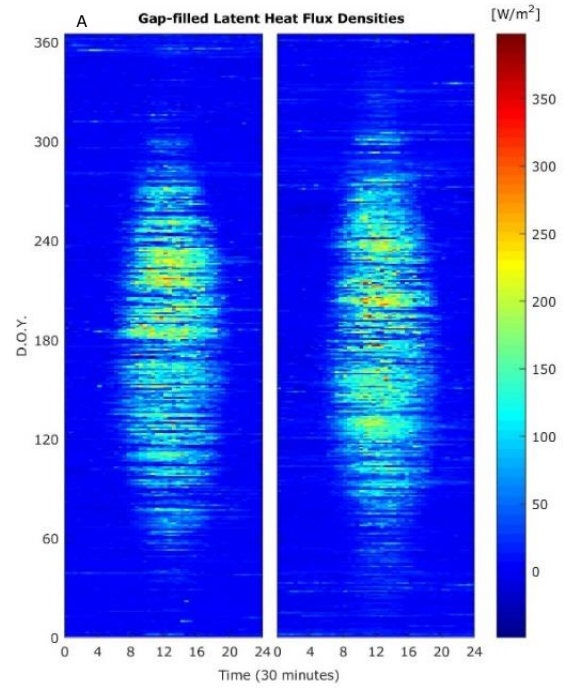


Figure 17. Latent heat flux densities (17A) after quality controlled gap-filling for 2015 (left) and 2016 (right) in W $m^{-2}$ illustrates diurnal and seasonal patterns. Evapotranspiration (17B) calculated from latent heat flux for 2015 (left) and 2016 (right) in millimeters of $H_2O$).

*4.3.3 Water Storage in the Ground and Soil*

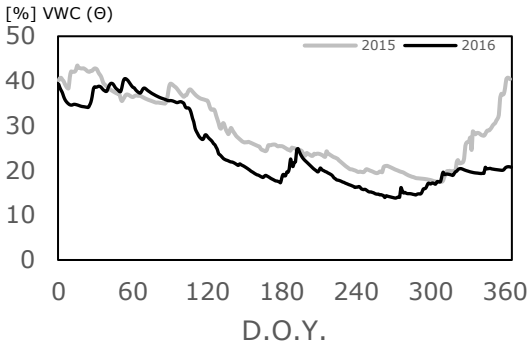


Figure 18. Change in daily volumetric water content (Θ) for the soil profile for 2015 (gray) and 2016 (black) in %.

The soil and groundwater received the brunt of the water shortage fallout when looking at the fluctuation shown in Figures 18, 19, and 20. Here we see a dip in soil water during the growing season for both years, but a lack in soil and ground water recharge late in 2016 as opposed to the steep recharge experienced in 2015..Figure 18 shows this best where the two years overlap one another in the figure to better portray the differences between the two study years. Groundwater (Figure 19), starting from July of 2015 a peak recharge occurring late in November, while such a drastic recharge is entirely lacking during the following year. The groundwater appeared to hit an all-time low in March of 2016. Because groundwater was not measured for the entirety of the study period, it is hard to

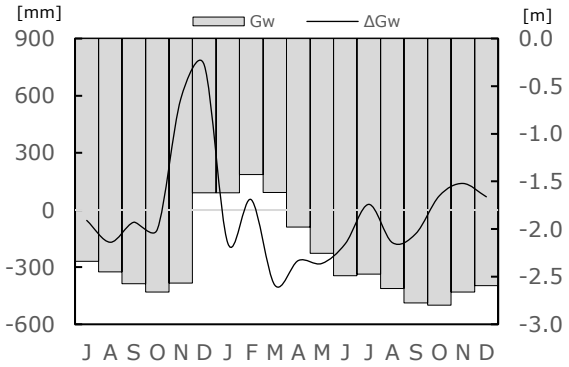


Figure 19. Change in ground water in millimeters and average monthly ground water level in meters below the ground surface from when measurements started in July of 2015 to the end of the study period.

say how greatly the drought of 2016 effected the water below the soil, but based off of Figure 19 alone, it appears that the drought did indeed have an effect on the recharge of depleted groundwater for the 2016 drought year.

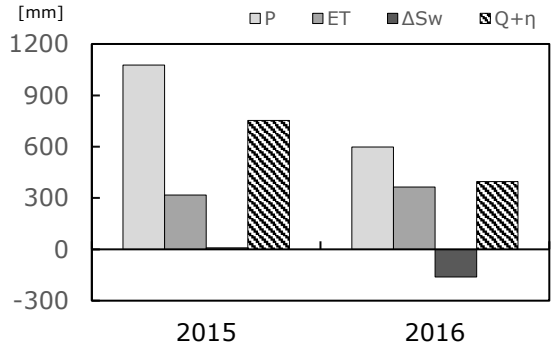


Figure 20. Annual breakdown of the water balance with totals for each of the four variables in millimeters.

### *4.3.4 Comprehensive Water Balance*

The four components of the water balance are best visualized by Figures 20, 21, and 22 where a time series of annual totals, individual cumulative sums, and monthly incremental sums, can be seen, respectively. While evapotranspiration performed relatively similarly, that was not the case for the remaining components of the water

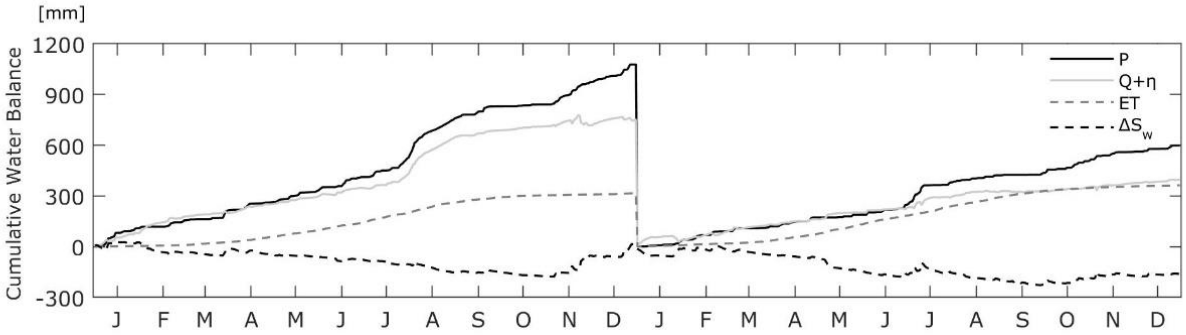


Figure 21. A comparative look at the water balance with daily running totals in millimeters for precipitation (P), evapotranspiration (ET), soil water storage ($\Delta S_w$), and discharge ($Q+\eta$).

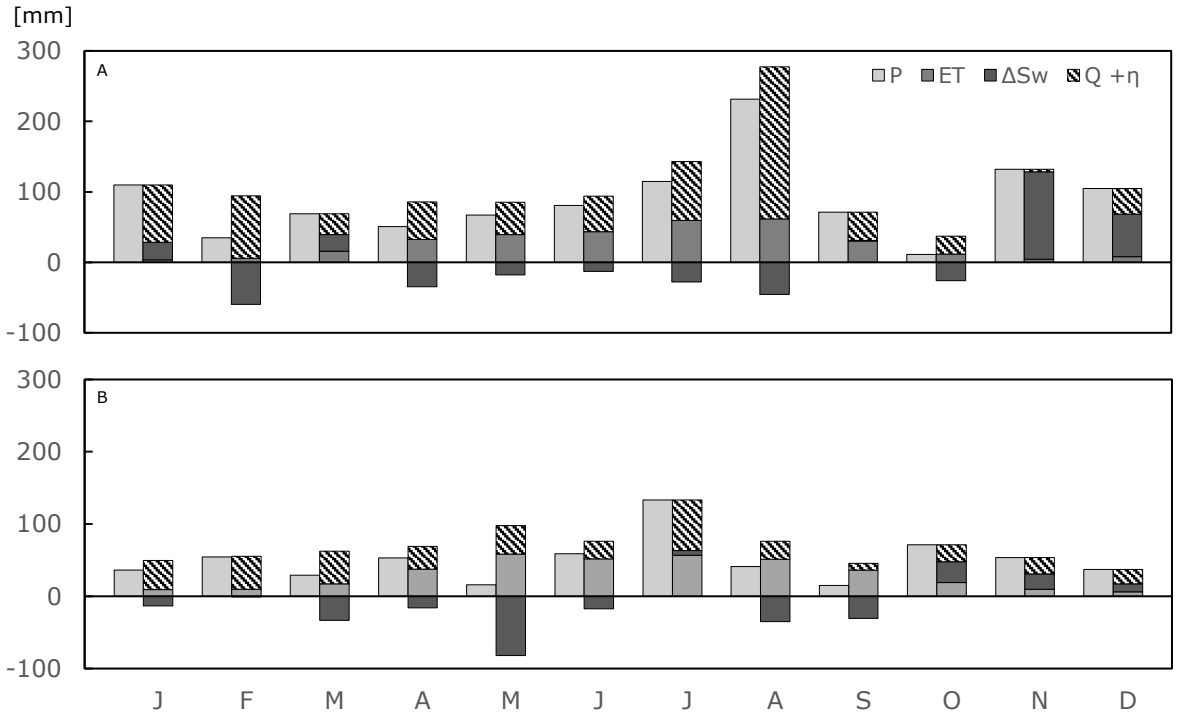


Figure 22. A top and bottom look at the monthly totals of precipitation, evapotranspiration, water discharge, and change in water storage for 2015 (22A) and 2016 (22B).

balance. With precipitation driving the entire water balance, there was a noteworthy decrease in $Q+\eta$ and $\Delta S_w$ during 2016 when precipitation events were less bountiful. During 2016 however, evapotranspiration increased. When looking at monthly and yearly cumulative sums, one can see that water storage was in the negative for much of 2016. Water discharge remained positive, though its sum was not as sizeable when looking at cumulative annual totals.

## 4.4 WUE and Carbon Fluxes

The ecosystem fluxes of carbon over the study period are seen in Figure 23. Here the daily totals of ecosystem exchanges of carbon, $CO_2$ fluxes, and evapotranspiration are expressed along with their running, cumulative totals for each year. The if starting from scratch each year, the forest became a carbon sink around mid-March each year. Both study years showed similar cumulative sums of the three ecosystem fluxes, though there were noticeable decreases in NEP in part of 2016 from May to July. Annual and entire study period sums are best explained in Table 4 for all parts of the carbon cycle explored in this study. There the annual flux differences between study years are quantified for comparison. Results for forest carbon and their effect on overall water use efficiency will be further explained.

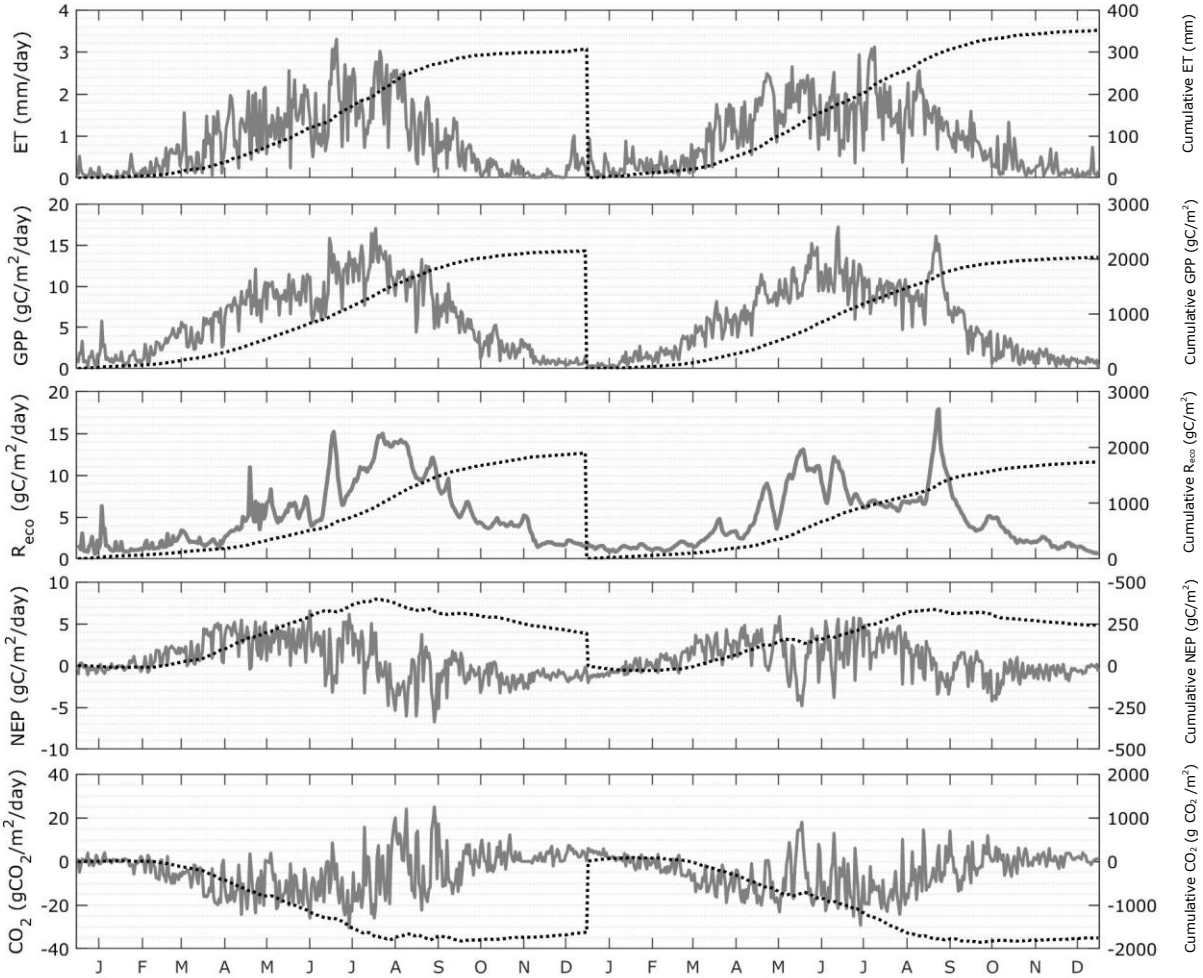


Figure 23. Daily rates of evapotranspiration, gross primary production, ecosystem respiration, net ecosystem production, and $CO_2$ flux scaled on the left y-axis, and daily running totals of evapotranspiration, gross primary production, ecosystem respiration, net ecosystem production, and $CO_2$ flux for each year scaled on the right y-axis.

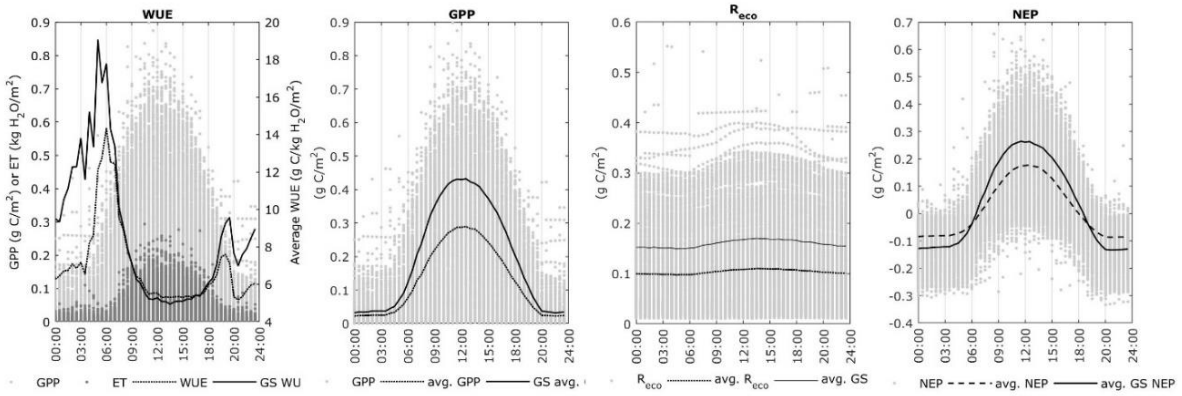


Figure 24. Diurnal cycles of water use efficiency individual components (ET (dark gray) in kilograms of water per square meter and GPP (light gray) in grams of carbon per square meter), carbon exchanges (GPP, NEP, and $R_{eco}$) in grams of carbon per square meter (light gray), and average diurnal water use efficiency (carbon to water) in grams of carbon per kilogram of water per square meter, GPP, $R_{eco}$, and NEP for the whole year (light line) and for the growing seasoning (dark line).

### *4.4.1 Cumulative Cycling of Forest Carbon*

As earlier mentioned, Figure 23 shows where forest carbon went during the entirety of the study period. The relationships between the three ecosystem exchanges can best be characterized there, with evapotranspiration and $CO_2$ fluxes also included to showcase the seasonal variations of these fluxes. Here the difference between partition estimated gross primary production (GPP) and ecosystem respiration ($R_{eco}$) explain the residual net ecosystem exchange (NEP). This difference serves as a tell for how well the given environment is at sequestering carbon for photosynthesis and later production of biomass. For 2016, there was both higher rates of GPP and $R_{eco}$, which resulted in a lower overall NEP for that year when compared with 2015 despite growth for 2016 being higher in terms of GPP than in 2015.

### *4.4.2 Daily Rhythms of Carbon Exchange, Evapotranspiration, and WUE*

Gross primary production and ecosystem respiration fluxes, and thus net ecosystem exchange were contingent on the climatic conditions present. GPP proved to be quite dependent on available light and ambient temperature (Figure 25) with light having a substantially stronger influence on these fluxes, as expressed with an $r^2$ of 0.81 and an RMSE of 0.042 grams carbon per square meter. Temperature also had a decent effect on ecosystem respiration with respiration taking off around five degrees Celsius. Rates of evapotranspiration indicated a solid dependence on the vapor pressure deficit present at the forest site. This relationship appeared to be the strongest of the four with an $r^2$ of 0.83 and an RMSE of 0.07 millimeters per second.

Diurnal patterns of evapotranspiration, gross primary production, ecosystem respiration, net ecosystem production, and water use efficiency showed seasonal variation between the growing season compared with the whole year. As expected, rates for all variables were highest during the growing season (Figure 24) meaning overall higher productivity during these months. Average diurnal peaks in water use efficiency for the growing season reached 21g C/kg $H_2O$ per square meter while it only reached ~14 for the whole year consisting of
the growing and winter seasons. These diurnal peaks in WUE can most likely be explained by a lag in daily evapotranspiration rates where GPP starts to increase in the morning before evapotranspiration rates start to speed up.

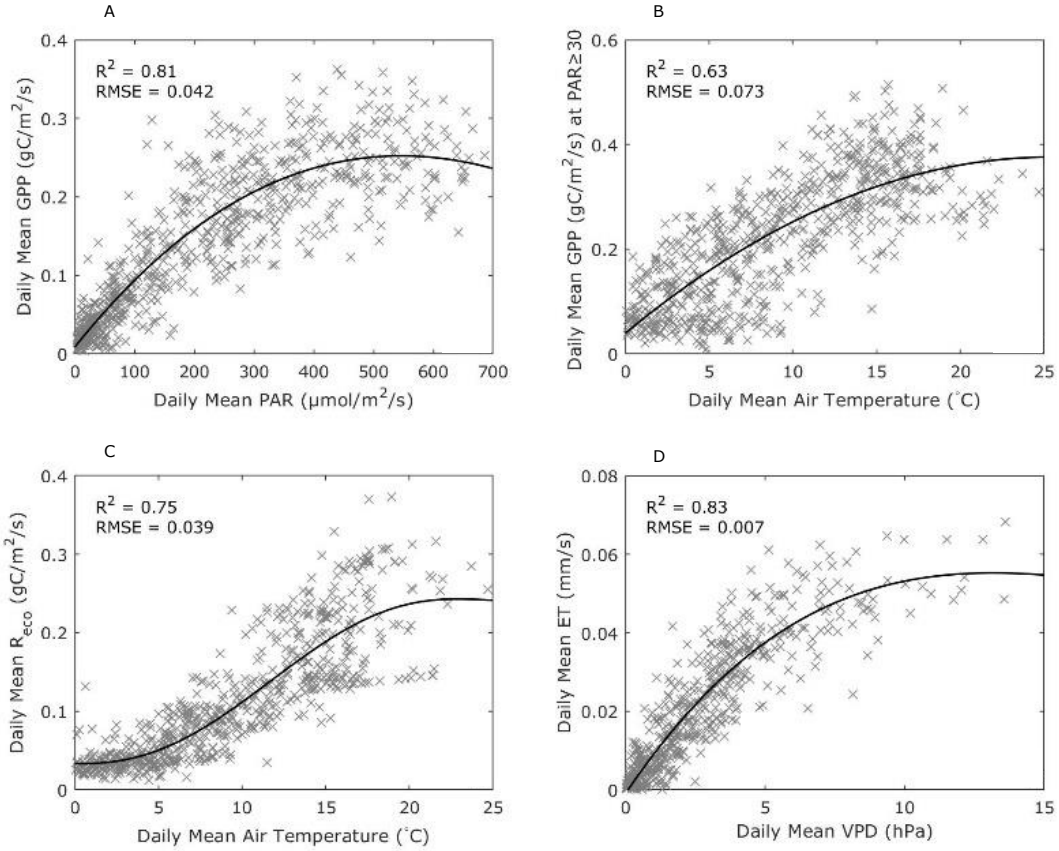


Figure 25. Relationship between daily rates of gross primary production and photosynthetically active radiation (25A), daily rates of gross primary production and ambient temperature (25B), and daily rates of ecosystem respiration and ambient temperature (25C), daily rates of evapotranspiration and vapor pressure deficit (25D).

### *4.4.3 Temporal WUE and Carbon Fluxes*

Sequestration of $CO_2$ (Figure 26) proved to be greatest during the daytime hours 8:00 and 17:00 throughout the growing season. The forest appeared to emit the most $CO_2$ during the late summer of 2015 in the morning and evening hours. Emissions during the summer of 2016 started earlier but did not reach the same level of peak emission as that of 2015. Nevertheless, the forest was able to capture more $CO_2$ in 2016 than 2015 (Table 4) despite emissions taking off earlier in 2016.

Monthly water use efficiency (Figure 27) shows a similar chronological curve for gross primary production and evapotranspiration. This association better

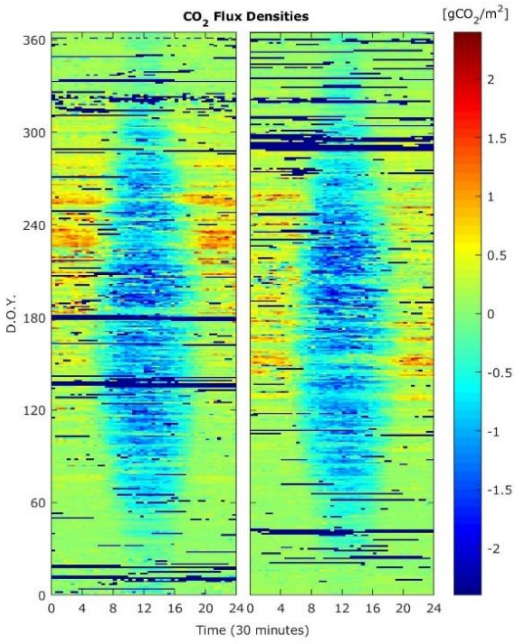


Figure 26. $CO_2$ flux densities for 2015 (left) and 2016 (right) in $gCO_2m^{-2}$ show diurnal and seasonal patterns of carbon sink and sourcing from the forest site.

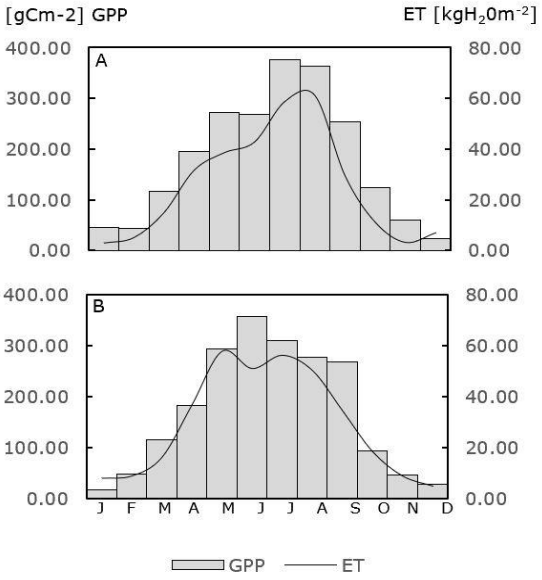


Figure 27. Monthly gross primary production in grams carbon per square meter (primary axis) with evapotranspiration in kilograms per square meter (secondary axis) for 2015 (27A) and 2016 (27B).

explains how these two processes are linked. June of 2016 appears to be the only month where evapotranspiration takes a dip, while gross primary production continues to increase.

A conclusive monthly quantities of WUE can be seen in Figure 28. Evapotranspiration on the x-axis was compared to GPP on the y-axis at a monthly scale. High correlation coefficients for monthly rates of WUE between ET and GPP at this larger temporal scale show an $r^2$ of 0.92. At a daily and 30-minute scale, this linear relationship between ET and GPP disintegrates where the best fit is curved and most of the points pooling towards the bottom left corner. The curved WUE at the daily scale showed an $r^2$ of 0.81 for 2015 and 0.75 for 2016 implying that only longer timescales show a true linear correlation whereas at the daily level, and

Table 4. Climatic and flux density information for each year of the study period with variable units, as well as two-year means and two-year totals for some of the aggregated variables for the entire duration of the study period.

| | 2015 | 2016 | Two-Year Mean | Two-Year Total |
|---|---|---|---|---|
| Mean Net Solar Radiation (W m-2) | 58.73 | 60.88 | 59.80 | -- |
| Mean Daytime Net Solar Radiation (W m-2) | 169.88 | 173.99 | 171.95 | -- |
| Mean Daytime Shortwave (W m-2) | 215.89 | 221.24 | 218.59 | -- |
| Mean Daytime Longwave (W m-2) | -46.05 | -47.32 | -46.69 | -- |
| Mean PAR (µmol m-2 s-1) | 209.87 | 220.63 | 215.26 | -- |
| Mean Daytime PAR (µmol m-2 s-1) | 459.41 | 477.58 | 468.56 | -- |
| Mean Annual Temperature (◦C) | 8.19 | 8.24 | 8.21 | -- |
| Mean Daytime Annual Temperature (◦C) | 12.69 | 11.17 | 11.60 | -- |
| Mean Nighttime Annual Temperature (◦C) | 7.28 | 5.73 | 6.67 | -- |
| Maximum Annual Temperature (◦C) | 30.36 | 27.95 | 29.16 | -- |
| Minimum Annual Temperature (◦C) | -8.51 | -13.37 | -10.94 | -- |
| Summer Days (max. temp. ≥ 25 ◦C) | 66.00 | 143.00 | 104.50 | -- |
| Mean Vapor Pressure Deficit (kPa) | 0.33 | 0.33 | 0.33 | -- |
| Mean Relative Air Humidity (%) | 86.78 | 85.96 | 86.36 | -- |
| Days with Precipitation ≥ 1.0 mm | 166.00 | 110.00 | 138.00 | -- |
| Days with Precipitation ≥ 10.0 mm | 29.00 | 13.00 | 21.00 | -- |
| Days with Snow Depth ≥ 1.0 mm | 56.00 | 84.00 | 70.00 | -- |
| Days with Snow Depth ≥ 10.0 mm | 9.00 | 21.00 | 15.00 | -- |
| Total Precipitation (mm year-1) | 1077.71 | 598.36 | 838.04 | 1676.07 |
| Total Q+η (mm year-1) | 752.86 | 396.50 | 574.68 | 1149.35 |
| Total ΔSw (mm year-1) | 8.14 | -161.44 | 26.64 | -153.30 |
| Total Evapotranspiration (mm year-1) | 316.72 | 363.30 | 340.01 | 680.02 |
| Total Gross Primary Production (gC m-2 year-1) | 2143.62 | 2027.43 | 2085.52 | 4171.04 |
| Total Ecosystem Respiration (gC m-2 year-1) | 1898.56 | 1736.34 | 1817.45 | 3634.90 |
| Total Net Ecosystem Production (g C m-2 year-1) | 245.06 | 291.09 | 217.96 | 435.91 |
| Total $CO_2$ Flux (g $CO_2$ m-2 year-1) | -1625.19 | -1751.92 | -1688.56 | -3377.11 |

even 30-minute scale, this is not quite the case. Looking at WUE in this way is a decent way of at least quantifying monthly rates, though intrinsic WUE would be more descriptive at finer temporal scales.

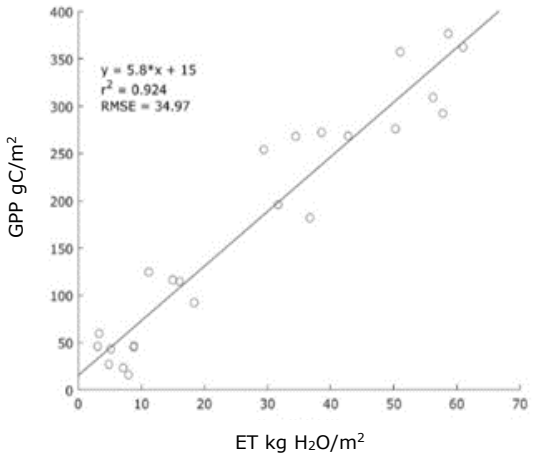


Figure 28. Gross primary production (y-axis) versus evapotranspiration (x-axis) showing monthly rates of water use efficiency for the entire study period (2015 and 2016).

# 5 DISCUSSION

Forest energy, water, and carbon dynamics for the ICOS Hyltemossa Research Station were evaluated for the duration of the study period ranging from January of 2015 to December of 2016. The energy balance, water balance, and ecosystem exchanges, namely in relation to water use efficiency, were studied. Some implications can disseminate from these results.

## 5.1 Forest Energy Balance

Firstly, the forest energy balance was thoroughly evaluated. The results indicated that measurements for the individual energy components were quite high before gap-filling and storage correction, however, the EBR for twenty-five percent lower than it needed to be for full closure. To solve this disparity the ground heat flux was corrected and the individual changes in storage energy were calculated. Upon evaluating the newly calibrated energy balance a twenty percent higher EBR was found. Despite a small reduction in correlation coefficients ($r^2$), the storage corrections still proved to be quite exceptional since the gap in the energy balance was initially quite high prior to correction (Barr et al. 2006, Wolf et al. 2008, Charuchittipan et al. 2014).

Additionally, the mean diurnal patterns of these different energy components were investigated. The largest daily contributors to the energy cycle were also easy to find when looking at daily energy rhythms (Oliphant et al. 2004, Moderow et al. 2009). This established a basic understanding of where energy moved throughout a typical day within this forest environment over the duration of the study period.

Friction velocities and windspeeds during different atmospheric stabilities in the daytime and nighttime conditions gave a robust understanding as to why better energy balance closure could not be achieved before energy storage correction (Fitzpatrick, Radić and Menounos 2017). A chronological look at the energy components revealed their seasonal trends and uncovered where there were shortcomings, specifically over and under flux estimations, in the EBR corrections. While the balance was close to one during the spring, summer, and fall months, trouble arose in the winter when corrections either under or overestimated the energy gap. Nevertheless, the energy storage corrections seemed to do a comparatively decent job of improving the imbalance in the energy cycle for these measured conditions. Seasonal trends for the energy balance and the individual energy components were within a reasonable range compared to previous studies in northern, water abundant latitudes, as was expected (Barr et al. 2006, Blanken et al. 1998, Nordbo et al. 2011).
The monthly Bowen ratios indicated an abundance of water during the non-growing season for 2015 and 2016, and greater sensible heat flux than latent heat flux during

the peak of the growing seasons. Monthly evaporative fractions indicated more than half of the turbulent fluxes were latent heat from July onward. This is in line with predictions made from previous research where sensible heat fluxes tended to be dominant during the growing seasons in environments that were typically water abundant (Bolinius, Jahnke and MacLeod 2016).

## 5.2 Forest Water Balance

The forest water balance presented some interesting findings since conditions varied so greatly between the study years. It was especially interesting to see how atypical results deviated from norms due to drought stress and other varying factors. While evapotranspiration only increased marginally for the drought year of 2016, its increase can likely be partially accredited to biological stress from dry soil conditions in the rooting zone where soil moisture is characteristically high for this environment (Wang et al. 2012). A reduction in annual discharge for the drought year was ascertained, and much lower monthly values for this term could be seen. With far less of a water surplus during the 2016 drought this could be expected. Soil water content often compensated for the noticeable shortage of water throughout the study period (Krzic et al. 2004). In late 2015 the soil storage was recharged, but for 2016 this was not the possible since there was a sizeable decrease in incoming precipitation. This resulted in a complete lack of water recharge until the late fall.

## 5.3 WUE and Ecosystem Exchanges of Carbon

Carbon fluxes in relation to ecosystem productivity were investigated for the purpose of defining forest growth efficacy for the study period. Both years showed similar outcomes with only slightly lower net primary productivity by the end of 2015. This dip in NEP, despite a higher annual total of GPP, can best be explained by the higher rates of $R_{eco}$ during that year. Lower total GPP for 2016 suggests a less efficient initial biological productivity during periods of prolonged environmental stress (Zhang et al. 2016, Beer et al. 2007). However, if environmental stressors, such as the 2016 drought, were to have a lasting effect on the carbon exchanges, annual rates of ecosystem respiration, and thus lower net ecosystem exchange, would have been higher than the previous year (Zhang et al. 2016). The drought likely had only a small effect on the carbon exchanges that year since NEP was actually higher during that time.

Ecosystem level water use efficiency suggested an effective water use to biomass growth relationship for the forest site when looking at longer temporal intervals at a basic level. For the purpose of larger temporal scales and for fundamental assessment of WUE, this appeared to work quite well where monthly values of WUE were in line with previous findings (Kuglitsch et al. 2008, Kwon et al. 2018, Scartazza et al. 2014, Beer et al. 2009). This relationship became less linear and predictable when accessed at the daily and 30-minute levels suggesting a need for more complex measures for modeling WUE that will better encapsulate more of the underlying mechanisms of these physiological processes at a smaller temporal scales (Medlyn et al. 2017, Medrano et al. 2015, Knauer et al. 2018). Average diurnal patterns of WUE fell within the typical range found in previous studies at comparable sites with similar vegetation (Kuglitsch et al. 2008).

## 5.4 Assumptions and Applications

Some general assumptions were made during the course of this study and should thus be noted. Firstly, it was assumed that the discrepancy in the energy balance could largely be explained by the unaccounted energy storage. Since the initial analysis of raw and gap-filled data showed high

statistical correlation coefficients, it was presumed that these measurements where accurate, but underestimated the turbulent fluxes. The results indicated that measurements and storage calculations of all of the individual energy components following correction were sufficient, so these assumptions are likely safe. While it is incredibly unlikely that these measurements were inaccurate it still should be mentioned since data was taken from a brand-new station where equipment was still being installed. Secondly, two of the storage equations had to be modified to fit available data. While this appears to have not elicited a problem when calculating these energy storage components, it could certainly explain the shortcomings of modeled storage results where oversimplification of these complex systems could posit a problem.

For the water balance it was implied that only four components of this complex cycle would suffice when evaluating the effects on this forest environment. While no clear problems seemed to arise from this, it should be noted that a more elaborate approach may be best be necessary when looking at the water balance in much finer detail or simply by itself.

For a broadscale approach when dealing with multiple systems, the parsimonious nature of the applications used in this study proved to be quite fruitful. Should there be a need for large scale ecosystem assessments, these methods should prove to enough to achieve similar research goals.

### 5.5 Future work

This study exposed the potential for a lot of research opportunities as it unfolded. While chronological scales were explored, unfortunately the spatial scale was entirely limited. Utilizing one or many spatial distributed model(s) for this forest system would be quite interesting and could potentially shed light on the spatial heterogeneity of this study site with regard to the energy balance, the water balance, and carbon exchanges that is simply not possible when solely analyzing the measurement data.
In addition, the drought experienced in 2016 pales in comparison to the one experienced in 2018 at this location. It would be informative to look at this data to see what effect this greater drought stress had on this typically water saturated environment. For the purpose of water use efficiency, taking a look at the plant level for carbon assimilation and transpiration would be beneficial when looking at finer time intervals or when trying to explain the intrinsic water use efficiency (Knauer et al. 2018, Yi et al. 2019, Medrano et al. 2015). This would require measurement data of leaf area index, which was recently added to tower instrumentation. Once that data is readily available, this can be explored.

Moving forward, it would also be enlightening to apply more complex storage calculations to see if they would perform better at correcting the energy imbalance. Another, more direct approach to energy closure problem would be to calculate imbalance ratios for turbulent sensible and latent heat fluxes where underestimation of these fluxes often occur due to lack of complete turbulent transport capture by most eddy covariance systems. This would most likely include at least some residual energy partitioning between the two turbulent fluxes, and as of now there are several, recently defined ways to achieve this (Charuchittipan et al. 2014, De Roo et al. 2018, Mauder et al. 2017, Stoy et al. 2013).

## 6 CONCLUSIONS

The complex and interconnected cycling of energy, water, and carbon were researched at a managed forest site in southern Sweden. The energy balance was evaluated for closure in order to validate later calculations of evapotranspiration for the water balance and water use efficiency. The carbon exchanges including: net primary

production, ecosystem respiration, gross primary production, and $CO_2$ fluxes were also described.

The modeled energy storage corrections resulted in favorable outcomes for energy balance closure where the EBR was improved by over twenty percent. Ideal conditions prior to modeled energy correction for energy balance closure happened during daytime hours when friction velocities were higher than 0.8 and windspeeds were greater than four meters per second during stable-neutral and unstable atmospheric stability. The individual nature of the energy components for the study conditions were examined, with the overall highest surface flux, aside from net radiation, being turbulent sensible heat flux and the largest contributor to energy storage being sensible heat storage. Diurnal patterns for the many radiation variables, evapotranspiration, and ecosystem exchanges were quantified, with most peaking around midday.

Water balance analysis indicated obvious effects from drought on the individual water components during 2016. This was especially apparent when looking at monthly temporal scales or finer where it is obvious water recharge did not occur until nearly end of 2016. This was further supported when comparing this drought year of 2016 with the 50-year average annual statistics. During this drought the hydrological components most effected were soil water storage and ground water storage. The drought however did not seem to negatively affect the ecosystem carbon exchanges or water use efficiency. The drought will likely need to be far more severe for an affect on these exchanges to be observed. Sequestration of $CO_2$ was surprisingly greater during the drought year.

Lastly, water use efficiency on a monthly scale and forest carbon exchange on several temporal scales at the ecosystem level were quantified for this study site. From this general conclusions about forest productivity were made, where the best times for forest productivity for both study years were during the growing seasons, as predicted. The forest was most water efficient and took up the most carbon during peak daylight hours of the growing season. This is most likely due to light and temperature dependence on these underlying processes.

# REFERENCES


Almeida, A. C., J. V. Soares, J. J. Landsberg & G. D. Rezende (2007) Growth and water balance of Eucalyptus grandis hybrid plantations in Brazil during a rotation for pulp production. *Forest Ecology and Management,* 251**,** 10-21. https://doi.org/10.1016/j.foreco.2007.06.009

Barr, A. G., K. Morgenstern, T. A. Black, J. H. McCaughey & Z. Nesic (2006) Surface energy balance closure by the eddy-covariance method above three boreal forest stands and implications for the measurement of the CO2 flux. *Agricultural and Forest Meteorology,* 140**,** 322-337. https://doi.org 10.1016/j.agrformet.2006.08.007

Beer, C., P. Ciais, M. Reichstein, D. Baldocchi, B. Law, D. Papale, J. Soussana, C. Ammann, N. Buchmann, D. Frank, D. Gianelle, I. Janssens, A. Knohl, B. Köstner, E. Moors, O. Roupsard, H. Verbeeck, T. Vesala, C. Williams & G. Wohlfahrt (2009) *Temporal and among-site variability of inherent water use efficiency at the ecosystem level*. https://doi.org/10.1029/2008GB003233

Beer, C., M. Reichstein, P. Ciais, G. D. Farquhar & D. Papale (2007) Mean annual GPP of Europe derived from its water balance. *Geophysical Research Letters,* 34. https://doi.org/10.1029/2006GL029006

Betts, R. A. (2000) Offset of the potential carbon sink from boreal forestation by decreases in surface albedo. *Nature (London)*, 187-190. https://doi.org/10.1038/35041545

Blanken, D., P. Den Hartog, G. Staebler, Ralf, Chen, Wenjun & M. Novak (1998) *Turbulent Flux Measurements Above and Below the Overstory of a Boreal Aspen Forest*. https://doi.org/10.1023/A:1001557022310

Bolinius, D. J., A. Jahnke & M. MacLeod (2016) Comparison of eddy covariance and modified Bowen ratio methods for measuring gas fluxes and implications for measuring fluxes of persistent organic pollutants. *Atmospheric Chemistry and Physics*, 5315. https://doi.org/10.5194/acp-16-5315-2016

Bonan, G. B. (2008) Forests and Climate Change: Forcings, Feedbacks, and the Climate Benefits of Forests. *Science*, 320, 1444-1449. https://doi.org/10.1126/science.1155121

Bredemeier, M. & S. Cohen (2011) *Forest Management and the Water Cycle*. Springer Netherlands. https://doi.org/10.1007/978-90-481-9834-4

Charuchittipan, D., W. Babel, M. Mauder, J.-P. Leps & T. Foken (2014) Extension of the Averaging Time in Eddy-Covariance Measurements and Its Effect on the Energy Balance Closure. *Boundary-Layer Meteorology*, 152, 303-327. https://doi.org/10.1007/s10546-014-9922-6

Coakley, A. J. (2003) Reflectance and albedo, surface. *Encyclopedia of Atmospheric Sciences*, 1914-1923. https://doi.org/10.1016/B0-12-227090-8/00069-5

De Roo, F., S. Zhang, S. Huq & M. Mauder (2018) A semi-empirical model of the energy balance closure in the surface layer. *PLOS ONE*, 13, e0209022. https://doi.org/10.1371/journal.pone.0209022

Diekmann, M. (1994) Deciduous forest vegetation in Boreo-nemoral Scandinavia. In *Acta phytogeographica Suecica*, 116 s. : ill., diagr., kartor, tab. ; 28 cm. Uppsala: Sv. växtgeografiska sällsk.

Fitzpatrick, N., V. Radić & B. Menounos (2017) Surface Energy Balance Closure and Turbulent Flux Parameterization on a Mid-Latitude Mountain Glacier, Purcell Mountains, Canada. *Frontiers in Earth Science*, 5. https://doi.org/10.3389/feart.2017.00067

Gower, S. T., J. G. Vogel, J. M. Norman, C. J. Kucharik, S. J. Steele & T. K. Stow (1997) Carbon distribution and aboveground net primary production in aspen, jack pine, and black spruce stands in Saskatchewan and Manitoba, Canada. *Journal of Geophysical Research: Atmospheres*, 102, 29029-29041. https://doi.org/10.1029/97JD02317

Hoekstra, A. Y. & P. Q. Hung (2003) Virtual water trade: A quantification of virtual water flows between nations in relation to international crop trade. *Water Science & Technology*, 49, 11, 203-209.

Ilvesniemi, H., J. LevuIa, R. Ojansuu, P. KoIari, L. KuImaIa, J. Pumpanen, S. Launiainen, T. VesaIa & E. Nikinmaa (2009) Long-term measurements of the carbon balance of a boreal Scots pine dominated forest ecosystem. *Boreal Environment Research*, 14, 731.

Jones, H., T. A. Black, R. S. Jassal, Z. Nesic, N. Grant, J. S. Bhatti & D. Sidders (2017) Water balance, surface conductance and water use efficiency of two young hybrid-poplar plantations in Canada's aspen parkland. *Agricultural and Forest*

*Meteorology*, 246**,** 256-271. https://doi.org/10.1016/j.agrformet.2017.04.007

Kljun, N., P. Calanca, M. W. Rotach & H. P. Schmid (2015) A simple two-dimensional parameterisation for Flux Footprint Prediction (FFP). *Geosci. Model Dev.*, 8**,** 3695-3713. https://doi.org/10.5194/gmd-8-3695-2015

Knauer, J., S. Zaehle, B. E. Medlyn, M. Reichstein, C. A. Williams, M. Migliavacca, M. G. De Kauwe, C. Werner, C. Keitel, P. Kolari, J. M. Limousin & M. L. Linderson (2018) Towards physiologically meaningful water-use efficiency estimates from eddy covariance data. *Global Change Biology*, 24**,** 694-710. https://doi.org/10.1111/gcb.13893

Kottek, M., J. Grieser, C. Beck, B. Rudolf & F. Rubel (2006) World Map of the Köppen-Geiger Climate Classification Updated. *Meteorologische Zeitschrift*, 15, 3, 259 – 263 https://doi.org/10.1127/0941-2948/2006/0130

Krzic, M., C. E. Bulmer, F. Teste, L. Dampier & S. Rahman (2004) Soil properties influencing compactability of forest soils in British Columbia. *Canadian Journal of Soil Science*, 84**,** 219. https://doi.org/10.4141/S03-056

Kuglitsch, F. G., M. Reichstein, C. Beer, A. Carrara, R. Ceulemans, A. Granier, I. A. Janssens, B. Koestner, A. Lindroth, D. Loustau, G. Matteucci, L. Montagnani, E. J. Moors, D. Papale, K. Pilegaard, S. Rambal, C. Rebmann, E. D. Schulze, G. Seufert, H. Verbeeck, T. Vesala, M. Aubinet, C. Bernhofer, T. Foken, T. Grünwald, B. Heinesch, W. Kutsch, T. Laurila, B. Longdoz, F. Miglietta, M. J. Sanz & R. Valentini (2008) Characterisation of ecosystem water-use efficiency of european forests from eddy covariance measurements. *Biogeosciences Discuss.*, 2008**,** 4481-4519. https://doi.org/10.5194/bgd-5-4481-2008

Kumar, V. & S. Jain (2008) Virtual water trade. *Current Science*, 93, 8, 1093-1099 https://doi.org/10.1529/biophysj.107.107482

Kwon, H., B. E. Law, C. K. Thomas & B. G. Johnson (2018) The influence of hydrological variability on inherent water use efficiency in forests of contrasting composition, age, and precipitation regimes in the Pacific Northwest. *Agricultural and Forest Meteorology*, 249**,** 488-500. https://doi.org/10.1016/j.agrformet.2017.08.006

Lewis, J. M. (1995) The Story behind the Bowen Ratio. *Bulletin of the American Meteorological Society*, 76**,** 2433-2444. https://doi.org/10.1175/1520-0477(1995)076<2433:TSBTBR>2.0.CO;2

Liu, H., B. Wang & C. Fu (2008) Relationships between surface albedo, soil thermal parameters and soil moisture in the semi-arid area of Tongyu, northeastern China. *Advances in Atmospheric Sciences*, 25**,** 757-764. https://doi.org/10.1007/s00376-008-0757-2

Luyssaert, S., E. D. Schulze, A. Börner, A. Knohl, D. Hessenmöller, B. E. Law, P. Ciais & J. Grace (2008) Old-growth forests as global carbon sinks. *Nature*, 455**,** 213. https://doi.org/10.1038/nature07276

Mauder, M., S. Genzel, J. Fu, R. Kiese, M. Soltani, R. Steinbrecher, M. Zeeman, T. Banerjee, F. De Roo & H. Kunstmann (2017) Evaluation of energy balance closure adjustment methods by independent evapotranspiration estimates from lysimeters and hydrological simulations. *Hydrological*

*Processes*, 32. https://doi.org/10.1002/hyp.11397

McCaughey, J. H. & W. L. Saxton (1988) Energy balance storage terms in a mixed forest. *Agricultural and Forest Meteorology*, 44**,** 1-18. https://doi.org/10.1016/0168-1923(88)90029-9

Medlyn, B. E., M. G. De Kauwe, Y.-S. Lin, J. Knauer, R. A. Duursma, C. A. Williams, A. Arneth, R. Clement, P. Isaac, J.-M. Limousin, M.-L. Linderson, P. Meir, N. Martin-StPaul & L. Wingate (2017) How do leaf and ecosystem measures of water-use efficiency compare?, *New Phytologist*, 216, 3, 758-770. https://doi.org/10.1111/nph.14626

Medrano, H., M. Tomás, S. Martorell, J. Flexas, E. Hernández, J. Rosselló, A. Pou, J.-M. Escalona & J. Bota (2015) From leaf to whole-plant water use efficiency (WUE) in complex canopies: Limitations of leaf WUE as a selection target. *The Crop Journal*, 3**,** 220-228. https://doi.org/10.1016/j.cj.2015.04.002

Moderow, U., M. Aubinet, C. Feigenwinter, O. Kolle, A. Lindroth, M. Mölder, L. Montagnani, C. Rebmann & C. Bernhofer (2009) Available energy and energy balance closure at four coniferous forest sites across Europe. *Theoretical and Applied Climatology*, 98, 3, 397-412. https://doi.org/10.1007/s00704-009-0175-0

Myneni, R. B., J. Dong, C. J. Tucker, R. K. Kaufmann, P. E. Kauppi, J. Liski, L. Zhou, V. Alexeyev & M. K. Hughes (2001) A large carbon sink in the woody biomass of Northern forests. *Proceedings of the National Academy of Sciences*, 98**,** 14784-14789. https://doi.org/10.1073/pnas.261555198

Nordbo, A., S. Launiainen, I. Mammarella, M. Leppäranta, J. Huotari, A. Ojala & T. Vesala (2011) Long-term energy flux measurements and energy balance over a small boreal lake using eddy covariance technique. *Journal of Geophysical Research: Atmospheres (1984–2012)*, 116. https://doi.org/10.1029/2010JD014542

Oliphant, A. J., C. S. B. Grimmond, H. N. Zutter, H. P. Schmid, H. B. Su, S. L. Scott, B. Offerle, J. C. Randolph & J. Ehman (2004) Heat storage and energy balance fluxes for a temperate deciduous forest. *Agricultural and Forest Meteorology*, 126**,** 185-201. https://doi.org/10.1016/j.agrformet.2004.07.003

Pan, X., Y. Liu, X. Fan & G. Gan (2017) Two energy balance closure approaches: applications and comparisons over an oasis-desert ecotone. *Journal of Arid Land*, 9**,** 51. https://doi.org/10.1007/s40333-016-0063-2

Pan, Y., R. A. Birdsey, J. Fang, R. Houghton, P. E. Kauppi, W. A. Kurz, O. L. Phillips, A. Shvidenko, S. L. Lewis, J. G. Canadell, P. Ciais, R. B. Jackson, S. W. Pacala, A. D. McGuire, S. Piao, A. Rautiainen, S. Sitch & D. Hayes (2011) A Large and Persistent Carbon Sink in the World's Forests. *Science*, 333**,** 988-993. https://doi.org/10.1126/science.1201609

Pidwirny, M. & S. Jones (2006) Actual and Potential Evapotranspiration. In *Fundamentals of Physical Geography*. University of British Columbia.

Ponton, S., L. B. Flanagan, K. P. Alstad, B. G. Johnson, K. Morgenstern, N. Kljun, T. A. Black & A. G. Barr (2006) Comparison of ecosystem water-use efficiency among Douglas-fir forest, aspen forest and grassland using eddy covariance and carbon isotope techniques. *Global*

*Change Biology*, 12**,** 294-310. https://doi.org/10.1111/j.1365-2486.2005.01103.x

Roxy, M. S., V. Sumithranand & G. Renuka (2014) *Estimation of soil moisture and its effect on soil thermal characteristics at Astronomical Observatory, Thiruvananthapuram, South Kerala*. Journal of Earth System Science. https://doi.org/10.1007/s12040-014-0509-x

Rubel, F. & M. Kottek (2010) Observed and projected climate shifts 1901-2100 depicted by world maps of the Köppen-Geiger climate classification. *Meteorologische Zeitschrift*, 19, 2, 135-141.https://doi.org/10.1127/0941-2948/2010/0430

Rubel, F. & M. Kottek (2011) Comments on: "The thermal zones of the Earth"" by Wladimir Köppen (1884). *Meteorologische Zeischrift*, 20, 3, 361 – 365. https://doi.org/10.1127/0941-2948/2011/0285

Sauer, T. J. & R. Horton (2005) Soil Heat Flux. *Encyclopedia of Soil Science, ch.* 7, 131-154. https://doi.org/10.1201/NOE0849338304.ch167

Scartazza, A., F. P. Vaccari, T. Bertolini, P. Di Tommasi, M. Lauteri, F. Miglietta & E. Brugnoli (2014) Comparing integrated stable isotope and eddy covariance estimates of water-use efficiency on a Mediterranean successional sequence. *Oecologia*, 176**,** 581-594. https://doi.org/10.1007/s00442-014-3027-2

Seibert, J., M. Jenicek, M. Huss & T. Ewen (2015) Chapter 4 - Snow and Ice in the Hydrosphere. In *Snow and Ice-Related Hazards, Risks and Disasters*, eds. J. F. Shroder, W. Haeberli & C. Whiteman, 99-137. Boston: Academic Press. https://doi.org/10.1016/B978-0-12-394849-6.00004-4

Sellers, P. J., R. E. Dickinson, D. A. Randall, A. K. Betts, F. G. Hall, J. A. Berry, G. J. Collatz, A. S. Denning, H. A. Mooney, C. A. Nobre, N. Sato, C. B. Field & A. Henderson-Sellers (1997) Modeling the Exchanges of Energy, Water, and Carbon Between Continents and the Atmosphere. *Science*, 275**,** 502-509. https://doi.org/10.1126/science.275.5299.502

Stoy, P. C., M. Mauder, T. Foken, B. Marcolla, E. Boegh, A. Ibrom, M. A. Arain, A. Arneth, M. Aurela, C. Bernhofer, A. Cescatti, E. Dellwik, P. Duce, D. Gianelle, E. van Gorsel, G. Kiely, A. Knohl, H. Margolis, H. McCaughey, L. Merbold, L. Montagnani, D. Papale, M. Reichstein, M. Saunders, P. Serrano-Ortiz, M. Sottocornola, D. Spano, F. Vaccari & A. Varlagin (2013) A data-driven analysis of energy balance closure across FLUXNET research sites: The role of landscape scale heterogeneity. *Agricultural and Forest Meteorology*, 171-172**,** 137-152. https://doi.org/10.1016/j.agrformet.2012.11.004

Tang, X., Z. Ding, H. Li, X. Li, J. Luo, J. Xie & D. Chen (2015) Characterizing ecosystem water-use efficiency of croplands with eddy covariance measurements and MODIS products. *Ecological Engineering*, 85**,** 212-217. https://doi.org/10.1016/j.ecoleng.2015.09.078

Teuling, A. (2011) Technical note: Towards a continuous classification of climate using bivariate colour mapping. *Hydrology and Earth System Science*, 15, 3071–3075. https://doi.org/10.5194/hess-15-3071-2011

Wang, S., B. J. Fu, G. Y. Gao, X. L. Yao & J. Zhou (2012) Soil moisture and

evapotranspiration of different land cover types in the Loess Plateau, China. *Hydrol. Earth Syst. Sci.,* 16**,** 2883-2892. https://doi.org/10.5194/hess-16-2883-2012

Wigley, T. M. L. & D. S. Schimel. (2009) The Carbon Cycle. *Cambridge University Press*. https://doi.org/10.1017/CBO9780511573095

Wolf, A., N. Saliendra, K. Akshalov, D. A. Johnson & E. Laca (2008) Effects of different eddy covariance correction schemes on energy balance closure and comparisons with the modified Bowen ratio system. *Agricultural and Forest Meteorology,* 148**,** 942-952. https://doi.org/10.1016/j.agrformet.2008.01.005

Wutzler, T., A. Lucas-Moffat, M. Migliavacca, J. Knauer, K. Sickel, L. Šigut, O. Menzer & M. Reichstein (2018) Basic and extensible post-processing of eddy covariance flux data with REddyProc. *Biogeosciences,* 15**,** 5015-5030. https://doi.org/10.5194/bg-15-5015-2018

Xuguang, T., L. Hengpeng, A. R. Desai, L. Juhua, T. E. Kolb, A. Olioso, X. Xibao, Y. Li, W. Kutsch, K. Pilegaard, B. Köstner & C. Ammann (2014) How is water-use efficiency of terrestrial ecosystems distributed and changing on Earth. *Scientific Reports***,** 1-11. https://doi.org/10.1038/srep07483

Yi, K., J. T. Maxwell, M. K. Wenzel, D. T. Roman, P. E. Sauer, R. P. Phillips & K. A. Novick (2019) Linking variation in intrinsic water-use efficiency to isohydricity: a comparison at multiple spatiotemporal scales. *New Phytologist,* 221**,** 195-208. https://doi.org/10.1111/nph.15384

Zhang, Y., X. Xiao, S. Zhou, P. Ciais, H. McCarthy & Y. Luo (2016) Canopy and physiological controls of GPP during drought and heat wave. *Geophysical Research Letters,* 43**,** 3325-3333. https://doi.org/10.1002/2016GL068501

# APPENDIX

Table A. Measured variables used from the ICOS Sweden Carbon Portal for the Hyltemossa site. Measurement information came directly from the ICOS website or from the metadata file downloaded with the measurement data.

| Variable | Measurement Type | Measurement Height (m) |
|---|---|---|
| Air pressure | Digital barometer | 1.5 |
| Air temperature | Temperature probes | 1, 4, 9, 14, 19, 24, 30, 40, 55, 70, 85, 100, 125, 148 |
| | Meteorological transmitter | 27 |
| Carbon dioxide ($CO_2$) | Gas analyzers | 1, 4, 9, 14, 19, 24, 30, 40, 55, 70, 85, 100, 125, 148 |
| | Flux system (IRGA, Sonic anemometer) | 27 |
| | Atmospheric system | 30, 70, 150 |
| Ecosystem fluxes (NEE, GPP, $R_{eco}$) | Flux system (IRGA, Sonic anemometer) | 27 |
| Ground water level | Pressure transducer (4x) | Close to soil profile |
| Heat fluxes (latent, sensible) | Flux system (IRGA, Sonic anemometer) | 27 |
| Photosynthetically active radiation (PAR) | Canopy transects (4x, 4 sensors each) | 1 |
| | Quantum sensor (incoming, outgoing) | 50 |
| | Sunshine sensor (diffuse, net incoming) | 150 |
| Precipitation | Rain gauge | 1.5 |
| Relative humidity | Meteorological transmitter | 27 |
| Snow depth | Sonic ranging sensor | 1.9 |
| Soil heat flux | Heat flux plates (4x) | -0.05 |
| Soil moisture | Theta probes (4 profiles) | 0 to -0.06 (vertical)<br>-0.05, -0.1, -0.3, -1.0 (horizontal) |
| Soil temperature | Temperature probes (4 profiles) | -0.02, -0.05, -0.1, -0.3, -1.0 |
| Solar radiation | Pyranometer (incoming) | 150 |
| | Net radiometer (incoming, outgoing) | 50 |
| Sun duration | Sunshine sensor | 150 |
| Surface temperature | Infrared Radiometer Sensor | 50 |
| Tree temperature | Temperature probes in spruce (3 levels, 4 sensors at N, S, E, W of each level) | ~3, ~9, ~15 |
| Water vapor | Gas analyzer | 1, 4, 9, 14, 19, 24, 30, 40, 55, 70, 85, 100, 125, 148 |
| | Flux system (IRGA, Sonic anemometer) | 27 |
| | Atmospheric system | 30, 70, 150 |
| Wind components | Flux system (Sonic anemometer) | 27 |

Table B. Variable names with variable symbols used in the paper including initial units and converted units for balancing calculations. Variables were designated as C for calculated. M for measured, or ** for constant value used.

| Variable | C, M, ** | Initial Units | Converted |
|---|---|---|---|
| Albedo | C | -- | -- |
| Photosynthetically Active Radiation (*PAR*) | M | µmol $m^{-2}$ $s^{-1}$ | -- |
| Relative Humidity (*RH*) | M | % | -- |
| Saturated Vapor Pressure ($e_s$) | C | hPa | kPa |
| Actual Vapor Pressure ($e_a$) | C | hPa | kPa |
| Vapor Pressure Deficit (*VPD*) | C | hPa | kPa |
| Air Temperature | M | ◦C | -- |
| Surface (Canopy) Temperature | M | ◦C | -- |
| Atmospheric Stability ($\zeta$) | C | -- | -- |
| Measurement Height ($z$) | M | m | -- |
| Surface Roughness | C | m | -- |
| Zero-plane Displacement Height ($d$) | C | m | -- |
| Obukhov Length ($L$) | C | m | -- |
| Friction Velocity ($u^*$) | M | m $s^{-1}$ | -- |
| Wind speed | M | m $s^{-1}$ | -- |
| Wind direction | M | Degrees | -- |
| Net Radiation ($R_n$) | M | W $m^{-2}$ | -- |
| Incoming Shortwave Radiation ($S\downarrow$) | M | W $m^{-2}$ | -- |
| Outgoing Shortwave Radiation ($S\uparrow$) | M | W $m^{-2}$ | -- |
| Incoming Longwave Radiation ($L\downarrow$) | M | W $m^{-2}$ | -- |
| Outgoing Longwave Radiation ($L\uparrow$) | M | W $m^{-2}$ | -- |
| Sensible Heat Flux ($H$) | M | W $m^{-2}$ | -- |
| Latent Heat Flux ($LE$) | M | W $m^{-2}$ | J $m^{-2}$ $s^{-1}$ |
| Surface Ground Heat Flux ($G_z$) | M | W $m^{-2}$ | -- |
| Ground Heat Storage ($G_s$) | C | W $m^{-2}$ | -- |
| Soil Volumetric Heat Capacity ($C_s$) | C | J $kg^{-1}$ $K^{-1}$ | -- |
| Average Soil Temperature ($T_s$) | M | ◦C | ◦K |
| Change in Soil Profile Depth ($\Delta z$) | C | m | -- |
| Energy Heat Storage ($J$) | C | J $m^{-2}$ $s^{-1}$ | W $m^{-2}$ |
| Sensible Heat Storage ($J_H$) | C | J $m^{-2}$ $s^{-1}$ | W $m^{-2}$ |
| Air Density ($\rho_a$) | C | g $m^{-3}$ | kg $m^{-3}$ |
| Specific Heat of Air ($c_p$) | C | J $kg^{-1}$ $K^{-1}$ | -- |
| Air Temperature Profile ($T_a$) | M | ◦C | ◦K |
| Change in Air Profile Height ($\Delta z$) | C | m | -- |
| Latent Heat Storage ($J_E$) | C | J $m^{-2}$ $s^{-1}$ | W $m^{-2}$ |
| Latent Heat of Vaporization ($\lambda$) | C | J $kg^{-1}$ | -- |
| Absolute Humidity, or Vapor Density, ($\rho_v$) | C | g $m^{-3}$ | kg $m^{-3}$ |
| Change in Vapor Profile Height ($\Delta z$) | C | m | -- |
| Vegetation (Stem) Storage ($J_s$) | C | J $m^{-2}$ $s^{-1}$ | W $m^{-2}$ |
| Wet biomass ($m_{veg}$) | C | kg $m^{-2}$ | -- |
| Specific Heat of Vegetation ($c_{veg}$) | ** | J $kg^{-1}$ $K^{-1}$ | -- |
| Change in Stem Temperature ($\Delta T_{veg}$) | M | ◦C | ◦K |

| | | | |
|---|---|---|---|
| Biochemical Heat Storage ($J_c$) | C | J $m^{-2}$ $s^{-1}$ | W $m^{-2}$ |
| Specific Energy for Photosynthetic Activity ($\mu$) | ** | J (kg $CO_2$)$^{-1}$ | J (g $CO_2$)$^{-1}$ |
| Bowen Ratio ($\beta$) | C | -- | -- |
| Evaporative Fraction (*EF*) | C | -- | -- |
| Energy Balance Ratio (*EBR*) | C | -- | -- |
| Precipitation (*P*) | M | mm | -- |
| Evapotranspiration (*ET*) | C | mm | -- |
| Change in Soil Water Storage ($\Delta S_w$) | C | mm | -- |
| Discharge with Error ($Q+\eta$) | C | mm | -- |
| Groundwater Depth | M | m | -- |
| Change in Groundwater Storage | C | m | mm |
| Snow Depth (*SD*) | M | m | -- |
| Snow Water Equivalent (*SWE*) | C | mm | -- |
| Snow Density | C | kg $m^{-3}$ | -- |
| Volumetric Water Content ($\Theta$) | M | % ($m^3$ $m^{-3}$) | -- |
| Net Ecosystem Exchange (*NEE*) | M | µmol $m^{-2}$ $s^{-1}$ | g C $m^{-2}$ $s^{-1}$ |
| Net Ecosystem Production (*NEP*) | C | µmol $m^{-2}$ $s^{-1}$ | g C $m^{-2}$ $s^{-1}$ |
| Gross Primary Production (*GPP*) | C | µmol $m^{-2}$ $s^{-1}$ | g C $m^{-2}$ $s^{-1}$ |
| Ecosystem Respiration ($R_{eco}$) | C | µmol $m^{-2}$ $s^{-1}$ | g C $m^{-2}$ $s^{-1}$ |
| Carbon Dioxide Flux | M | µmol $m^{-2}$ $s^{-1}$ | g CO2 $m^{-2}$ $s^{-1}$ |
| Inherent Water Use Efficiency (*WUE*) | C | g C $m^{-2}$ (kg H2O $m^{-2}$)$^{-1}$ | -- |